Journal of Print and Media Technology Research

Scientific contributions

Journal of Print and Media Technology Research

A PEER-REVIEWED QUARTERLY

PUBLISHED BY

A mission statement

To meet the need for a high quality scientific publishing platform in its field, the International Association of Research Organizations for the Information, Media and Graphic Arts Industries is publishing a quarterly peer-reviewed research journal.

The journal is fostering multidisciplinary research and scholarly discussion on scientific and technical issues in the field of graphic arts and media communication, thereby advancing scientific research, knowledge creation, and industry development. Its aim is to be the leading international scientific journal in the field, offering publishing opportunities and serving as a forum for knowledge exchange between all those interested in contributing to or learning from research in this field.

By regularly publishing peer-reviewed, high quality research articles, position papers, surveys, and case studies as well as review articles and topical communications, the journal is promoting original research, international collaboration, and the exchange of ideas and know-how. It also provides a multidisciplinary discussion on research issues within the field and on the effects of new scientific and technical developments on society, industry, and the individual. Thus, it intends to serve the entire research community as well as the global graphic arts and media industry.

The journal is covering fundamental and applied aspects of at least, but not limited to, the following topics:

Printing technology and related processes
⊕ Conventional and special printing
⊕ Packaging
⊕ Fuel cells and other printed functionality
⊕ Printing on biomaterials
⊕ Textile and fabric printing
⊕ Printed decorations
⊕ Materials science
⊕ Process control

Premedia technology and processes
⊕ Colour reproduction and colour management
⊕ Image and reproduction quality
⊕ Image carriers (physical and virtual)
⊕ Workflow and management

Emerging media and future trends
⊕ Media industry developments
⊕ Developing media communications value systems
⊕ Online and mobile media development
⊕ Cross-media publishing

Social impact
⊕ Media in a sustainable society
⊕ Environmental issues and sustainability
⊕ Consumer perception and media use
⊕ Social trends and their impact on media

Submissions to the Journal

Submissions are invited at any time and, if meeting the criteria for publication, will be rapidly submitted to peer-review and carefully evaluated, selected and edited. Once accepted and edited, the papers will be published as soon as possible.

✉ Contact the Editorial office: journal@iarigai.org

Journal of Print and Media Technology Research

3-2018

September 2018

Contents

A letter from the Editor

Gorazd Golob
Editor-in-Chief
E-mail: gorazd.golob@jpmtr.org
journal@iarigai.org

This issue of the Journal is being created right before the joint conferences of iarigai and IC, two important international print and media associations, involving academic, research and educational organizations, as well as industrial enterprises and institutes. Expectations are optimistic, as the organizers announced the participation of numerous recognized researchers and experts who will present their latest results and achievements.

The results of previous research, partly already presented at the conferences, are also published in this third 2018 issue of the Journal. Two research papers are the work of the same authors, but they cover quite different topics, although both of them are related to the quality of color reproduction in the print proces. The first paper deals with the new spectral trapping model in halftoning, which represents an improvement of well-known and widely used halftoning in pre-press workflow, based on the improved Demichel and Neugebauer mathematical models. Considering trapping given as a color difference in halftoned patches of secondary and tertiary colors, a model with a potential for improving the quality of four-color reproduction in the press is shown.

The second paper deals with an improved automated CtP calibration model for offset printing. With the proposed enhancement, it is possible to correct the rendering of the printing forms in view of the changes in the materials used for printing and in the printing machine settings. Based on the spectrophotometric measurements of a relatively small number of control patches, sufficient data are obtained to make changes in the settings of RIP, which is an integral part of the CtP Workflow system, to achieve the optimal rendering of the printing plates under given print conditions.

The third research article shows the process of optimizing the production of printed chipless RFID tag, as a necessary condition for the implementation of this modern coding system in wide use, potentially even as a replacement or upgrade of established barcodes and 2D codes. The emphasis is on sintering methods that, under normal conditions of use (wireless communication quality, speed, price), can help to achieve technically appropriate and also market-acceptable production of RFID tags, and the results presented are promising.

This time the Topicalities bring an overview of the latest standards adopted by ISO TC 130 – Graphic technology and news on international research activities and the new Master of Engineering degree in Printed Intelligence. The review of new books covers the fields of image quality and typography as well as materials, photovoltaics, and packaging. A new edition of the book Introduction to Graphic Communication is presented, which also gives an interactive experience to the

reader, however, with some initial issues. Associate editor Markéta Držková (marketa.drzkova@jpmtr.org), who edited and composed the Topicalities, also chose three interesting doctoral dissertations, even from the universities less known in our research community. At TU Darmstadt, IDD, Maximillian Klammer defended the thesis on the use of CCD line camera as a measuring device for color and stereoscopic measurement. David Joseph Finn successfully defended the thesis in the field of inkjet printing of nanomaterials on flexible temperature sensitive substrates at Trinity College, Dublin. The third presented doctoral thesis by Nouran Yehia Adly, defended at RWTH Aachen University, is also based on a research on inkjet printing, this time for the production of electrochemical devices for bioelectronics.

The overview of conferences and symposia in the autumn period begins with already mentioned 45th International iarigai Conference and the 50th International Circle Conference, which both take place in Warsaw, where the Department of Printing Technology of the Warsaw University of Technology celebrates the 50th anniversary. We could expect a number of interesting new contributions and some of the authors already expressed their interest in publishing full, revised and extended papers in the Journal, after the Conferences.

During the course of the two conferences, activities will also be undertaken to improve the content and recognition of the Journal as one of the key channels for publishing the results of scientific and research work in the area it covers. The results should be visible in the forthcoming issues.

Ljubljana, September 2018

A novel spectral trapping model for color halftones

Sasan Gooran[1] and *Shahram Hauck*[2]

[1] Dept. of Science and Technology, Linköping University,
    Campus Norrköping, 601 74 Norrköping, Sweden   sasan.gooran@liu.se
[2] Dept. of Informatics and Media, Beuth University of Applied Sciences Berlin,
    Luxemburger Straße 10, 13353 Berlin, Germany   shauck@beuth-hochschule.de

Abstract

The amount of trapping has a great impact on the gray balance and color reproduction of printed products. The conventional trapping models are print density based and give percentage values to estimate the effect of trapping. In an earlier research, a spectral trapping model was proposed, that defines the trapping effect as the ΔE^*_{ab} colorimetric differences between the real ink overlap (measurements) and the ideal ink overlap. All the trapping models proposed so far, however, only calculate the trapping value for full-tone (solid) ink overlap. As the trapping value for full-tone ink overlap could be overestimating the actual ink trapping effect for halftones, it is important to be able to also approximate the trapping value of color halftones. Furthermore, for a detailed gray balance shift analysis, there is a need to estimate the trapping effect for specific color halftones. In the present paper, we propose a novel spectral trapping model that delivers the trapping value as ΔE^*_{ab} color difference for color halftones taking into account secondary and tertiary ink overlap. The results of the experiments show that the trapping values for color halftones are much smaller than the corresponding trapping value at full tone. The trapping value of halftones, besides other common quality parameters, should still be considered if some quality inaccuracy, such as gray balance shift, occurs in a print production.

Keywords: ink trapping, halftoning, gray balance, color difference (ΔE^*_{ab}), printing quality

1. Introduction

In a multicolor offset printing machine, the process inks (KCMY) are printed consecutively on the substrate in one printing unit after the other. The dots in different ink units are printed either isolated or partly or completely overprinted and the overprinted inks are printed wet on wet. The thickness or the amount of the second printed ink on the first one is not the same as when the second ink is printed on the paper, which makes the ink overlap not be ideal. This phenomenon is called trapping. Trapping varies due to different parameters such as ink temperature, dampening, printing speed, etc. Trapping affects the gray balance and the color appearance (secondary and tertiary colors) of the printed products. Therefore, it is very important to have an explicit value for measuring trapping.

There are different conventional trapping models, such as Preucil (1953), Brunner (Du Pont, 1979), Ritz (1996), Hamilton (1986) and Viggiano and Prakhya (2008), which are named after their inventors, and give a trapping value based on the amount of the second printed ink on top of the first one in percent. There is also a spectral trapping model proposed in literature that presents the trapping value as ΔE^*_{ab} color difference (Hauck and Gooran, 2011; 2013). Hence, the latter model delivers more useful and meaningful trapping value for the press machine operators than the conventional trapping models. As also been shown in Hauck and Gooran (2011), the dynamic range of this model is larger than the conventional trapping models. However, all trapping models proposed so far, including the aforementioned spectral trapping model, only calculate the trapping value for full-tone (solid) ink overlap. However, the trapping value for full-tone ink overlap could be overestimating the actual ink trapping that might occur for halftones. Furthermore, for a detailed gray balance shift analysis, there is a need to estimate the trapping effect for specific color halftones.

In the present paper, we propose a novel spectral trapping model that delivers the trapping value as ΔE^*_{ab} color difference for color halftones and takes into account secondary and tertiary ink overlap. We start with a short introduction to the previously published

spectral trapping model for full-tone ink overlap, following with a description of the proposed spectral trapping model for color halftones. The results of the model are presented and discussed and finally, summary and conclusion of the paper are given.

2. The spectral trapping model for full-tone ink overlap

The spectral trapping model for full-tone ink overlap is based on the reflectance spectra and presents the trapping value as the ΔE^*_{ab} color difference (Hauck and Gooran, 2011). The color difference is computed between the CIELAB values of the ideal ink overlap and the measured (real) ink overlap. For a single printed ink, for example cyan or magenta in Figure 1, the reflectance spectra $R_c(\lambda)$ and $R_m(\lambda)$ can be calculated by Equations [1] and [2], respectively.

$$R_c(\lambda) = T_c^2(\lambda) \cdot R_p(\lambda) \qquad [1]$$

$$R_m(\lambda) = T_m^2(\lambda) \cdot R_p(\lambda) \qquad [2]$$

Here $R_p(\lambda)$, $T_c(\lambda)$ and $T_m(\lambda)$ denote the reflectance of the paper, the transmittance of full-tone cyan and the transmittance of full-tone magenta, respectively. Note that the incoming light passes through the ink layer twice before being reflected back, and that is why the transmittances are squared in Equation [1] and [2]. The reflectance of the overlapped inks, $R_b^{ideal}(\lambda)$, assuming ideal ink overlap, in this case magenta printed on cyan (giving blue) as shown to the right in Figure 1, is calculated by Equation [3].

$$R_b^{ideal}(\lambda) = T_c^2(\lambda) \cdot T_m^2(\lambda) \cdot R_p(\lambda) \qquad [3]$$

Here $R_b^{ideal}(\lambda)$ represents the spectral reflectance of full-tone blue (cyan + magenta), assuming ideal ink overlap.

Inserting Equations [1] and [2] into Equation [3] gives Equation [4], which is the calculated overlapped spectral reflectance based on the reflectance of the single inks printed on paper and the reflectance of the paper, assuming ideal ink overlap has occurred.

$$R_b^{ideal}(\lambda) = \frac{R_c(\lambda) \cdot R_m(\lambda)}{R_p(\lambda)} \qquad [4]$$

For the calculation of trapping, both the measured, i.e. $R_b^{measured}(\lambda)$, and the ideal overlapped spectral reflectance, i.e. $R_b^{ideal}(\lambda)$ from Equation [4], are needed. These two reflectance spectra are therefore converted to CIELAB values. The trapping value in this trapping model is defined as the ΔE^*_{ab} color difference between these two CIELAB values. In this paper, ΔE^*_{ab} according to the CIE 1976 color difference formula (Equation [5]) is used. However, other color difference formulas, such as ΔE^*_{94} or ΔE^*_{00}, can also be used.

$$\Delta E^*_{ab} = \sqrt{(\Delta L^*)^2 + (\Delta a^*)^2 + (\Delta b^*)^2} \qquad [5]$$

The trapping value for red and green can be calculated correspondingly.

For tertiary ink overlap, i.e. CMY, the proposed model needs to include three inks. Since the yellow ink is usually and according to ISO 12647-2:2013 (International Organization for Standardization, 2013) printed on top of cyan and magenta inks (giving blue), the tertiary ink overlap can be considered as full-tone blue and full-tone yellow ink overlap. Therefore, Equation [6] shows the ideal spectral reflectance for full-tone CMY.

$$R_{cmy}^{measured}(\lambda) = \frac{R_b(\lambda) \cdot R_y(\lambda)}{R_p(\lambda)} \qquad [6]$$

The trapping value is calculated, as before, by Equation [5] between the CIELAB values of the ideal full-tone CMY ink overlap and the real (measured) full-tone CMY ink overlap.

It has been shown in Hauck and Gooran (2011) that the correlation factors between the trapping value according to ΔE^*_{ab} and the Ritz (1996) and Preucil (1953) models, being the most known and important conventional trapping models, are 93 % and 96 %, respectively. Furthermore, it has also been shown that the dynamic range of the proposed spectral trapping model for full-tone ink overlap is larger than that of both the Preucil and the Ritz model, which makes the spectral model even more useful for the press operators.
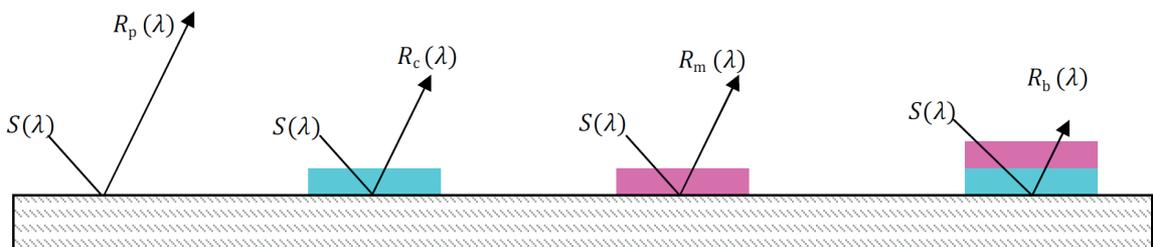

Figure 1: A schematic of a full-tone ink print, from left: paper, cyan, magenta and ideal ink overlap

3. The novel spectral trapping model for color halftones

As discussed in Section 2, all trapping models proposed so far, calculate the trapping value only for full-tone ink overlap. As will be shown later in Section 4, the trapping values calculated for full-tone ink overlap overestimate the actual trapping occurring in color halftones. Furthermore, for a better analysis of printing quality, a thorough understanding of trapping value for halftones can be very useful. For example, the gray balance shift, which is one of the most important quality criterion in color printing, can be better analyzed if the trapping value for halftones are also known in addition to dot gain and other basic parameters.

Like in the spectral trapping model for full-tone ink overlap, in the proposed model the trapping value is defined as the color difference ΔE^*_{ab} between the ideal and the real ink overlap. Since the proposed model is supposed to be used for color halftones having different primary ink combinations, there is a need for a color prediction model to approximate the reflectance spectra of a color halftone. The used color prediction model is described in the following subsection.

3.1 The used color prediction model

Neugebauer equation (Neugebauer, 1937), Equation [7], is commonly used to approximate the average reflectance spectra of a color halftone.

$$R_{average}(\lambda) = \sum_i a_i R_i(\lambda) \qquad [7]$$

where i denotes the so-called Neugebauer primaries (NPs): the substrate with no ink, single ink and multi-ink overlap combinations, summing up to a total of 2^m primaries, m being the total ink number; $R_i(\lambda)$ is the spectral reflectance of each NP at full-tone, a_i is the corresponding fractional ink area coverage of the NPs and $R_{average}(\lambda)$ is the calculated/approximated spectral reflectance of the color halftone. Assuming a semi-stochastic ink overlap behavior between primary inks, Demichel equations (Demichel, 1924) can be used to calculate a_i. However, Neugebauer equation presented in Equation [7] does not take into account the effect of dot gain if a_i coefficients are calculated using the reference (commanded) ink coverage of the primary inks in the digital bitmap. Therefore, the model we propose to use as the color prediction model starts by first calculating the effective dot coverage using Murray-Davies formula (Murray, 1936), Equation [8].

$$R_{MD}(\lambda) = aR_i(\lambda) + (1-a)R_p(\lambda) \qquad [8]$$

where R_p, R_i and a denote the reflectance spectrum of the paper, the reflectance spectrum of the full-tone ink,

and the coverage of the ink, respectively. If $R_{MD}(\lambda)$ is replaced by the real (measured) reflectance spectra of a halftone in Equation [8], the effective ink coverage of the ink can be calculated by Equation [9].

$$a_{eff}(\lambda) = \frac{R_{measured}(\lambda) - R_p(\lambda)}{R_i(\lambda) - R_p(\lambda)} \qquad [9]$$

Therefore, in the proposed model, Equation [9] is used to find the effective coverage for the primary inks, i.e. cyan, magenta and yellow. Notice that, in our proposed model, as seen in Equation [9], the effective coverages are wavelength dependent and all multiplications and divisions are performed element-wise. Assuming the reflectance spectra being measured from 400 nm to 700 nm with a step of 10 nm, all spectra and thereby the effective coverages are 1 × 31 vectors. This is something that differs this used color prediction model from many of the other color prediction models.

After the effective coverages of the primary inks have been calculated, Demichel equations can be used to find the coverage of the Neugebauer primaries (NPs), see Equation [10].

$$\begin{cases} a_p(\lambda) = (1 - a_{eff}^c(\lambda)) \cdot (1 - a_{eff}^m(\lambda)) \cdot (1 - a_{eff}^y(\lambda)) \\ a_c(\lambda) = (a_{eff}^c(\lambda)) \cdot (1 - a_{eff}^m(\lambda)) \cdot (1 - a_{eff}^y(\lambda)) \\ a_m(\lambda) = (1 - a_{eff}^c(\lambda)) \cdot (a_{eff}^m(\lambda)) \cdot (1 - a_{eff}^y(\lambda)) \\ a_y(\lambda) = (1 - a_{eff}^c(\lambda)) \cdot (1 - a_{eff}^m(\lambda)) \cdot (a_{eff}^y(\lambda)) \\ a_r(\lambda) = (1 - a_{eff}^c(\lambda)) \cdot (a_{eff}^m(\lambda)) \cdot (a_{eff}^y(\lambda)) \\ a_g(\lambda) = (a_{eff}^c(\lambda)) \cdot (1 - a_{eff}^m(\lambda)) \cdot (a_{eff}^y(\lambda)) \\ a_b(\lambda) = (a_{eff}^c(\lambda)) \cdot (a_{eff}^m(\lambda)) \cdot (1 - a_{eff}^y(\lambda)) \\ a_k(\lambda) = (a_{eff}^c(\lambda)) \cdot (a_{eff}^m(\lambda)) \cdot (a_{eff}^y(\lambda)) \end{cases} \qquad [10]$$

where, indices p, c, m, y, r, g, b and k denote the following eight NPs, paper, cyan, magenta, yellow, red (magenta + yellow), green (cyan + yellow), blue (cyan + magenta) and black (cyan + magenta + yellow), respectively. The effective coverages $a_{eff}^c(\lambda)$, $a_{eff}^m(\lambda)$ and $a_{eff}^y(\lambda)$ are calculated using Equation [9].

Notice that Equation [10] is written for three primary inks, giving $2^3 = 8$ NPs. If two primary inks were involved, only the coverages of 4 NPs were needed to be calculated by Demichel equations. Notice also that, as discussed above, even in Equation [10], the multiplications are performed element-by-element and therefore the coverage of NPs are also wavelength dependent and represented by vectors. The coverage of NPs calculated in Equation [10] can now be used in Neugebauer equation (Equation [7]) to approximate the reflectance spectrum of a color halftone, see Equation [11].

$$\begin{aligned} R_{halftone}^{model}(\lambda) = a_p(\lambda)R_p(\lambda) + a_c(\lambda)R_c(\lambda) + a_m(\lambda)R_m(\lambda) \\ + a_y(\lambda)R_y(\lambda) + a_r(\lambda)R_r(\lambda) + a_g(\lambda)R_g(\lambda) \\ + a_b(\lambda)R_b(\lambda) + a_k(\lambda)R_{cmy}(\lambda) \end{aligned} \qquad [11]$$

where $a_i(\lambda)$ is the effective coverage of NPs calculated using Equation [10], and $R_i(\lambda)$ is the reflectance

spectrum of the NPs at full tone. Notice again that the multiplications in Equation [11] are also performed element-by-element.

Before we use this model to approximate the trapping value described in Section 3.2, the accuracy of the proposed model needs to be examined. Since the proposed trapping model is supposed to be practically useful, it is important that the number of patches (i.e. training samples) to be measured is limited. Therefore, as will be discussed in more detail in Section 4.2, to examine the model we have chosen three color halftones using different CMY ink coverage combinations, namely (a_c = 25 %, a_m = 18.4 %, a_y = 18.6 %), (a_c = 50 %, a_m = 40.9 %, a_y = 40.1 %) and (a_c = 75 %, a_m = 68.9 %, a_y = 69.9 %). For each halftone, we firstly used Equation [9] to calculate the effective ink coverage for each primary ink. Then, Equation [10] was used to find the ink coverage for all eight NPs and thereafter Equation [11] was used to approximate/calculate the spectral reflectance of the halftone. The ΔE^*_{ab} color differences between the CIELAB values of this calculated and the measured reflectance spectrum of the color halftones were calculated, being 0.52, 0.94 and 2.72 for these three color halftones, respectively, giving the well acceptable average of 1.39 ΔE^*_{ab}. As expected, the color prediction model is less accurate for darker halftones, giving the higher value of 2.72 ΔE^*_{ab}. This color difference is still acceptable, especially when considering the fact that only 17 patches were needed to be measured to predict the colors. For these calculations, we needed to measure eight patches to be used in Equation [11]. These eight patches are paper (1 patch), the primary inks at full tone (3 patches), the secondary inks at full tone (3 patches), and the tertiary ink (CMY) at full tone (1 patch). We also needed to measure nine patches to find the effective coverage for primary inks by Equation [9]. These nine patches are halftones of cyan at 25 %, 50 % and 75 % (3 patches), halftones of magenta at 18.4 %, 40.9 % and 68.9 % (3 patches), and halftones of yellow at 18.6 %, 40.1 % and 69.9 % (3 patches).

Due to the fact that not many patches are needed to be measured and also the simplicity of the proposed color prediction model, this model is used in this paper to predict the color of halftones and thereby approximating the trapping value, which is described in the following subsection.

3.2 Approximating trapping value of color halftones

In order to approximate the trapping value of color halftones, like in the spectral trapping model for full-tone inks described in Section 2, two different ink overlaps have to be taken into account, namely ideal ink

overlap and real ink overlap. Therefore, for red, green, blue and black (cyan + magenta + yellow) halftones, the model presented in Section 3.1 is used to calculate the spectral reflectance of the halftones. By setting the measured reflectance spectra of the paper, primary ($R_c(\lambda)$, $R_m(\lambda)$, $R_y(\lambda)$), secondary ($R_r(\lambda)$, $R_g(\lambda)$, $R_b(\lambda)$), and tertiary ($R_{cmy}(\lambda)$) inks at full tone in the right-hand side of Equation [11], the real reflectance spectrum of a halftone is approximated, which is denoted by $R^{real}_{halftone}(\lambda)$.

Then, by setting

$$R_r(\lambda) = R_r^{ideal}(\lambda) = \frac{R_m(\lambda) \cdot R_y(\lambda)}{R_p(\lambda)} \text{ (similar to Equation [4]),}$$

$$R_g(\lambda) = R_g^{ideal}(\lambda) = \frac{R_c(\lambda) \cdot R_y(\lambda)}{R_p(\lambda)} \text{ (similar to Equation [4]),}$$

$$R_b(\lambda) = R_b^{ideal}(\lambda) = \frac{R_c(\lambda) \cdot R_m(\lambda)}{R_p(\lambda)} \text{ (Equation [4]), and}$$

$$R_{cmy}(\lambda) = R_{cmy}^{ideal}(\lambda) = \frac{R_b(\lambda) \cdot R_y(\lambda)}{R_p(\lambda)} \text{ (Equation [6])}$$

in the right-hand side of Equation [11], the ideal reflectance spectrum, called $R^{ideal}_{halftone}(\lambda)$ is also calculated for the same halftone. The ΔE^*_{ab} color difference between the CIELAB values of $R^{real}_{halftone}(\lambda)$ and $R^{ideal}_{halftone}(\lambda)$ is now calculated and used as an approximation of the trapping value of the color halftone.

4. Results and discussion

In order to study the trapping effect on color halftones, a number of experiments were carried out. The experiments were done using a sheet-fed offset printing machine (Speedmaster 74) and high glossy coated papers on both sides; AM halftoning at lpi = 150 and dpi = 2 400 was used. The color channels were halftoned at different angles, ensuring a semi-stochastic ink overlap behavior between primary inks, for which Demichel equations can be used.

In this section the results of the approximation of the trapping values for full-tone ink overlap, and also color halftones, as well as an analysis of the results are given.

4.1 Full-tone ink trapping value

Table 1: The trapping value for full-tone R, G, B and CMY ink overlap

Trapping value	R	G	B	CMY
ΔE^*_{ab}	14.7	7.2	13.9	17.4

For full-tone red (R), green (G) and blue (B) trapping values, Equation [4] (or its correspondence for R and G), was used to calculate the ideal spectral reflectance.

By calculating ΔE^*_{ab} color difference between the ideal and the measured reflectance spectra, the trapping values for full-tone R, G and B were calculated, see Table 1.

For black full tone (cyan + magenta + yellow, CMY), Equation [6] was used to calculate the ideal spectral reflectance, which was compared to the measured full-tone CMY, as discussed above.

As expected, the ink trapping value for full-tone CMY (tertiary) is higher than those for full-tone secondary ink overlap. Furthermore, it can be noticed that the trapping value for green (yellow on cyan) is lower than the rest, which was also expected. The reason is that the print processing time between the cyan (printing unit 2) and yellow (printing unit 4) printing units, is longer than the other two combinations which are printed in consecutive printing units. Therefore, in the full-tone green, the cyan ink has more time to be dried before the second ink (yellow) is printed on top of it, which causes a smaller trapping effect.

4.2 Trapping value of color halftones

By using the spectral trapping model for halftones presented in Section 3, we calculated the trapping value for four different color halftones of R (MY), G (CY), B (CM) and CMY, respectively. The tonal value of each ink coverage combination making the halftones was taken from the proposed tonal values for gray balance and gray reproduction presented in Table A.1 in Annex A to ISO 12647-2:2013 (International Organization for Standardization, 2013), which is also shown in Table 2.

Table 2: The used tonal values for R, G, B and CMY halftones

Color	Quarter tone (%)	Mid tone (%)	Three quarter tone (%)	Full tone (solid) (%)
C	0.250	0.500	0.750	1.000
M	0.184	0.409	0.689	1.000
Y	0.186	0.401	0.699	1.000

For example, a quarter tone B (CM) halftone in our experiments means a halftone consisting of 25.0 % C and 18.4 % M. A mid-tone CMY halftone, for example, means a halftone consisting of 50 % C, 40.9 % M and 40.1 % Y. The ink coverage combinations of other halftones were chosen accordingly.

As observed in Table 3, the trapping value for halftones are much less than their counterparts for full tones. This means that the trapping values for full-tone prints overestimate the actual trapping effect on halftone prints. Another observation is that the trapping value increases with increasing tonal value. The reason is

that with increasing tonal value, the ink overlapping areas also increase, resulting in increased trapping effect. As also mentioned in Section 4.1 and as also expected, the trapping values for all CMY halftones are larger than the trapping values of their corresponding two-ink overlaps (R, G and B halftones). The trapping values for G halftones are smaller than the trapping values for other halftones, meaning that they are following the same trend as those for full-tone, discussed in Section 4.1.

Table 3 shows the ΔE^*_{ab} trapping value for halftone R, G, B and CMY at four different tone ranges specified above.

Table 3: The ΔE^*_{ab} trapping value for halftone and full-tone R, G, B and CMY

Color	Quarter tone	Mid tone	Three quarter tone	Full tone (solid)
R	0.1	0.7	2.8	14.7
G	0.1	0.5	2.0	7.2
B	0.2	1.1	3.4	13.9
CMY	0.3	1.9	6.6	17.4

Recall from Section 3.1 that only 17 patches were needed to be measured to estimate the trapping values of these color halftones.

4.3 Analysis of ink trapping effect on printed color halftones

For evaluation and analysis of gray balance at different tonal values, normally the dot gain for C, M and Y halftones and the CIELAB values of the CMY halftones and full-tone CMY print are used. Besides these quality criteria, the trapping values for halftones, can also be used for a better understanding and analysis of halftone color prints and specifically gray balance. Therefore, we propose that during the print process calibration (CtP calibration) according to ISO 12647-2:2013 (International Organization for Standardization, 2013) or PSO-calibration (Belz, 2012; 2016) the trapping value is also noted along with other parameters such as dot gain, etc. If in a print production some quality inaccuracy, such as gray balance shift, occurs, besides other common quality parameters, the trapping value should also be considered. If other parameters are inside the acceptance range but trapping value has increased compared to the value noted at the print process calibration, then the parameters affecting trapping should be checked. The most important parameters affecting trapping are ink temperature, dampening, printing speed, and rheology of the inks (Hauck, 2015).

In the fourth row of Table 3, the ΔE^*_{ab} trapping value of four different CMY halftones were shown. In order to
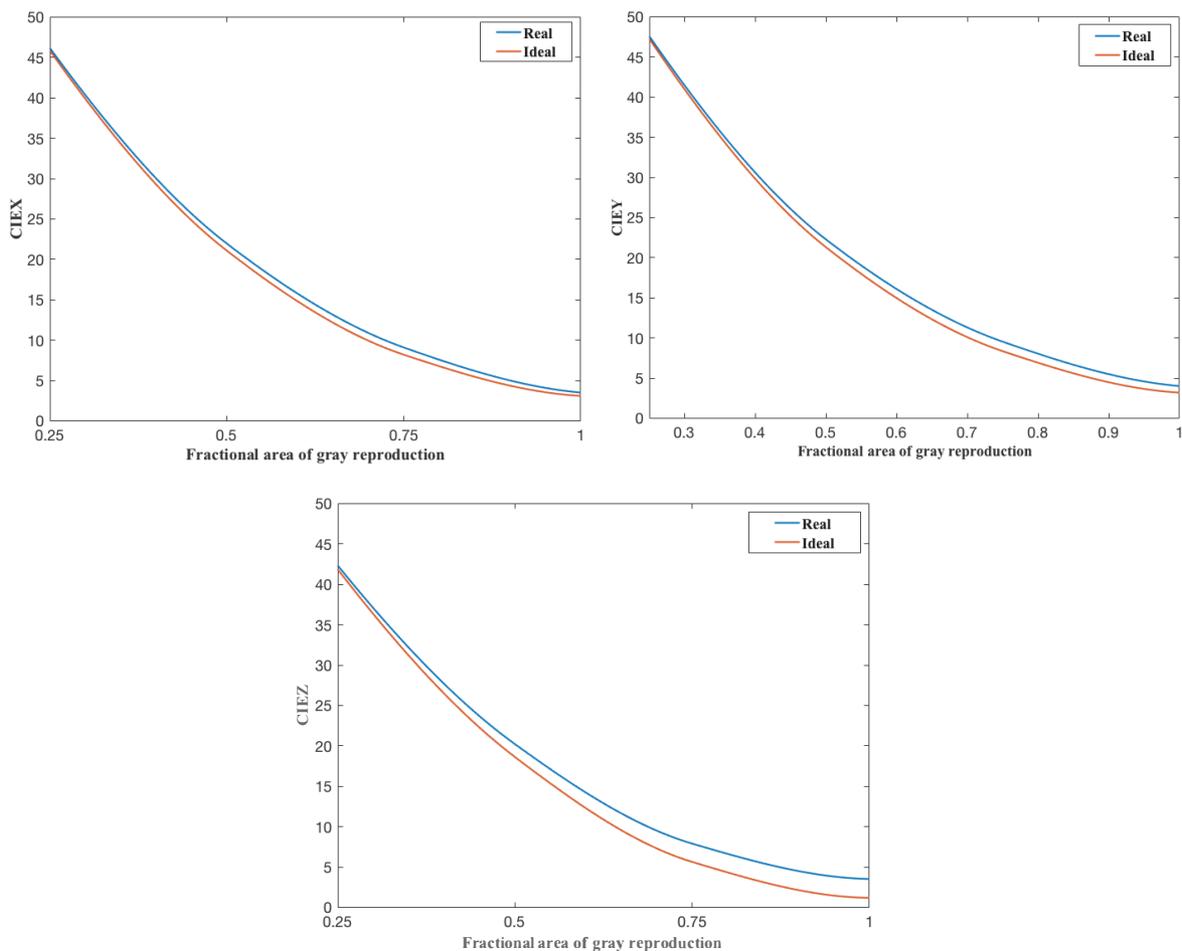
*Figure 2: Interpolated CIE X, Y and Z values of CMY halftones for real and ideal ink overlap
at tonal values according to Table 2*

conduct a better analysis of trapping effect, the CIEXYZ values for real (measured data which include ink trapping) and ideal CMY ink overlap at the four tonal values shown in Table 2 were calculated. They were then interpolated and shown in Figure 2. The first observation by noticing these curves is that the CIE X, Y and Z values for the ideal ink overlap are all smaller than those of the real ink overlap. This means that, trapping effect makes the halftones brighter, which was expected. Another observation is that, the difference in the CIE Z values between real and ideal ink overlap is more than the difference in the CIE X and CIE Y values. This means that trapping causes the halftones to be more blueish. The reason is that, trapping mainly causes the overprinted ink (in this case yellow) to be thinner than in ideal case, which makes the print less yellowish (and thereby more blueish) and also brighter.

By using these curves, it is also possible to find an approximation of the trapping value at any tonal value for gray reproduction. This can be done, by firstly collecting the CIE *X*, *Y*, *Z* color values from the real and ideal curves in Figure 2 at that specific tonal value, and then by converting them to CIELAB values it is possible to calculate the ΔE^*_{ab} trapping value for that specific halftone.

5. Summary and conclusion

All trapping models proposed in literature so far have delivered the trapping value considering full-tone (solid) ink overlap. In this paper, a novel spectral trapping model for color halftones has been proposed. The model delivers the trapping value as the ΔE^*_{ab} color difference taking into account both the ideal ink overlap (full ink trapping) and the real ink overlap (measurement). The results of our experiments show that the trapping values of color halftones are much smaller than those of their counterparts at full-tone, but still not negligible for some halftones. The proposed model is practically useful because it is simple to implement and it doesn't need many training samples to be measured. Despite the simplicity, the model is still general

S. Gooran and S. Hauck – J. Print Media Technol. Res. 7(2018)3, 107–113

113

and can be used to approximate the trapping value of any color halftone having arbitrary ink coverage combinations.

We believe that for a better analysis of printing quality, a thorough understanding of trapping effect on halftones can be very useful. Therefore, besides other parameters such as dot gain, the effect of the trapping on print quality has to be studied. The proposed model helps the print machine manufacturers and print machine operators to gain a better understanding of trapping effect on different color halftones.

References

Belz, H., 2012. *ProcessStandard Offsetdruck: Wirtschaftlich und Farbsicher produzieren von der Datenerzeugung bis zum Auflagendruck*. Wiesbaden: bvdm.

Belz, H., 2016. *ProcessStandard Offsetdruck: Wirtschaftlich und Farbsicher produzieren von der Datenerzeugung bis zum Auflagendruck: Revision 2016*. Wiesbaden: bvdm.

Demichel, M.E., 1924. *Le Procédé*, 1924, Vol. 26(3), pp. 17–21, 26–27.

Du Pont, 1979. *Eurostandard Cromalin*. Frankfurt am Main: Felix Brunner.

Hamilton, J.F., 1986. A new ink-trap formula for newsprint. In: *TAGA 1986 Proceedings of annual conference. Valley Forge*. Rochester, New York: Technical Association of the Graphic Arts, pp. 158–165.

Hauck, S. and Gooran S., 2011. An alternative computational method of trapping for the print machine operators. In: *TAGA 63rd Annual Technical Conference*. Pittsburgh, Pennsylvania, 6–9 March 2011. Sewickley: Technical Association of Graphic Arts, pp. 51–52.

Hauck, S., and Gooran, S., 2013. Investigation of the effect of ink penetration and gloss on a proposed spectral trapping model for high quality glossy coated paper. *Journal of Print and Media Technology Research*, 2(4), pp. 235–244.

Hauck, S., 2015. *Automated CtP calibration system for offset printing – dot gain compensation, register variation and trapping evaluation*. PhD Dissertation. Linköping University.

International Organization for Standardization, 2013. *ISO 12647-2:2013 Graphic technology – Process control for the production of halftone color separations, proof and production prints – Part 2: Offset lithographic processes*. Geneva: ISO.

Murray, A., 1936. Monochrome reproduction in photoengraving. *Journal of The Franklin Institute – Engineering and Applied Mathematics*, 221(6), pp. 721–744.

Neugebauer, H.E.J., 1937. Die theoretischen Grundlagen des Mehrfarbenbuchdrucks. *Zeitschrift für wissenschaftliche Photographie, Photophysik und Photochemie*, 36(4), pp. 73–89.

Preucil, F., 1953. Color hue and ink transfer – their relation to perfect reproduction. In: *Proceedings of the 5th annual technical meeting – Technical Association of Graphic Arts*. Rochester, New York: Technical Association of Graphic Arts, pp. 102–110.

Ritz, A., 1996. A halftone treatment for obtaining multi-colour ink film trapping values. *Professional Printer*, 40(5), pp. 11–17.

Viggiano, J.A.S. and Prakhya, S.H., 2008. Prediction of overprint spectra using trapping models: a feasibility study. In: *RIT TAGA Student Chapter*, 34. Rochester: RIT, pp. 113–133.

S. Hauck and S. Gooran – J. Print Media Technol. Res. 7(2018)3, 115–125

115

Automated CtP calibration system in an offset printing workflow

Shahram Hauck[1] *and Sasan Gooran*[2]

[1] Dept. of Informatics and Media, Beuth University of Applied Sciences Berlin,
    Luxemburger Straße 10, 13353 Berlin, Germany   shauck@beuth-hochschule.de

[2] Dept. of Science and Technology, Linköping University,
    Campus Norrköping, 601 74 Norrköping, Sweden   sasgo@itn.liu.se

Abstract

Although offset printing has been and still is the most common printing technology for color print productions, its print productions are subject to variations due to environmental and process parameters. Therefore, it is very important to frequently control the print production quality criteria in order to make the process predictable, reproducible and stable. One of the most important parts in a modern industrial offset printing process is Computer to Plate (CtP), used for printing plate production. One of the most important quality criteria for printing is to control the dot gain level. It is crucial to have the dot gain level within an acceptable range, defined by ISO 12647-2:2013. This is done by dot gain compensation methods in the Raster Image Processor (RIP). Dot gain compensation, which is also referred to as CtP calibration is, however, a complicated task in offset printing because of the huge number of parameters affecting dot gain. The conventional CtP calibration methods for an offset printing process, which are very time and resource demanding and hence expensive, mostly use one to five dot gain correction curves as the maximum. The proposed CtP calibration method in this paper calibrates the dot gain according to ISO 12647-2:2013 recommendations fully automatically parallel to the print production. Besides that, there is no limitation of the number of the needed dot gain correction curves. This automated CtP calibration method, which is much more efficient and economically beneficial compared to conventional CtP calibration methods, also makes the printing production very accurate in terms of dot gain value.

Keywords: workflow control system, printing process variables, ISO 12647-2:2013, dot gain compensation, raster image processor

1. Introduction and background

One of the most important parts in a modern industrial offset printing is Computer to Plate (CtP), which exposes the printing plate directly from digital data. In the modern industrial offset printing, the printing plate has been made by CtP since the end of the 20th century.

The calibration of computer to plate means correcting dot gain shift by generating a compensation curve. The CtP calibration is not to be misunderstood with linearization of a CtP. The linearization of a CtP is the adjustment of laser beams (focus, intensity, etc.) and the setting and adjusting of the plate developing machine. The CtP linearization has to be checked regularly (e.g. weekly) and is done independently of CtP calibration (Kipphan, 2001). The calibration of CtP is necessary for a precise color prediction in the printing process

(Mittelhaus, 2000); CtP calibration is also a necessary basic condition for a successful color management process (Homann, 2007). Since color management is not a part of CtP calibration it is out of the scope of this paper.

One of the most important quality criteria for printing is to control the dot gain level. Dot gain refers to an important phenomenon that causes the printed elements to appear larger than their reference size sent to the CtP. Dot gain shift is defined as the difference between the printed tone value and the ISO recommended tone value for print. The ISO recommended tone values for print and their tolerances for an offset printing process are described in ISO 12642-2:2013 (International Organization for Standardization, 2013). Therefore, CtP calibration means correcting dot gain shift by a generated compensation curve. The Dot Gain Compensation Curves (DGCCs) are used in the Raster Image Processor

(RIP) of a CtP. ISO 12647-2:2013 describes eight different Print Conditions (PCs). For each PC eight print substrates (PS1 to PS8) are possible. Five different Tone Value Increases (TVIs), named A to E are also assigned, dependent on the printing substrate and the halftoning method (FM or AM screening). The description in ISO 12647-2:2013 is very clear, easy and understandable, but keeping the dot gain within the demanded range for all the productions is very difficult in practice. There are two main reasons for that. Firstly, the needed test prints for generating a DGCC are very time demanding and expensive. Secondly, the offset printing is not stable and the generated DGCC should be controlled and if necessary renewed and replaced regularly. Because of that, printing companies usually work only with a few DGCCs but the combination of consumables and printing processes result in a high number of different printing workflows requiring a higher number of DGGCs. Any printing workflow is more or less different to the other one and demands its specific DGCCs in order to be in the range of ISO 12647-2:2013 recommended tone value.

In literature, three different methods for calibration are identified. While two of them make use of one dimensional transforms for each printing channel, the third method makes use of multi-dimensional transforms in the form of International Color Consortium (ICC) device link profiles (McDowell, 2007). The method recommended to be used in the proposed automated CtP calibration system in this paper belongs to the first category, which uses the TVI (dot gain) curves.

In Gu (2008), some methods regarding linear adjustment of digital proof and CtP output process for packaging offset have been discussed. Leng (2009) has reported a research on characteristic curve for CtP, to provide reference for dot gain compensation of CtP plate making. Fogra has also published their own guidelines for CtP acceptance test (Schmitt, Ondrusch and Rauh, 2010). There have also been patents proposing different methods for dot gain (or CtP) calibration (Fisher, Koifman and Weiss, 2003; Hendersson, 2013; Hauck, 2012; 2013).

Although the CtP calibration has been discussed in many reports and scientific articles, it is still a complicated and time demanding task in practice. One of the reasons is that there are many different parameters, such as printing substrates, inks, dampening solutions, plates, temperature, humidity, etc., that affect the quality of the offset print productions. In practice, some of these parameters are grouped (for example printing substrates) to reduce the number of combinations. This might cause the dot gain to be out of the allowed range. A suggested solution is to use a practically applicable automated CtP calibration system that takes into account all combinations of parameters affecting dot gain.

This paper describes a novel automated CtP calibration system for a modern and economical offset printing process. The proposed system is a concept, which produces, renews and uses the exactly needed DGCCs, taking into account all consumables and all offset printing processes. All the DGCCs for the different consumables and offset printing processes are saved in a data base. The Workflow Control System (WCS) in a control unit controls the workflow. The concept is based on three requirements which are necessary for this automated CtP calibration system.

First in this paper, the three necessary requirements for the automated CtP calibration are explained, in Section 2. Other important requirements such as the Print Quality Program, available measuring devices, etc., are also explained. In Section 3, the work principle of the WCS is described. For defining a print job according to the ISO definition for the printed tone values the WCS has to make a choice between generating a new DGCC or just using an existing DGCC or renewing an existing DGCC. From now on in this paper, these three choices are called DGCC-Generation, DGCC-Usage, and DGCC-Renewal.

2. Necessary requirements for automated CtP calibration

The requirements for realizing an automated CtP calibration system can be divided into three groups, to fulfill the minimum requirements on an automated CtP calibration system for a modern and economical offset printing process. The first requirement is the controlling of print quality conditions in order to avoid variation in the printing process. The automated CtP calibration system is designed to use and renew DGCCs parallel to the printing production and without a separate print test. There are two types of methods to generate DGCCs, iterative (Hauck, 2013) and non-iterative ones (Hauck, 2012). The iterative methods for generating the DGCCs require a number of iterations, which make them inappropriate to be used in the automated CtP calibration system. Hence the second requirement is a non-iterative method to generate DGCCs. The third requirement is the workflow networking, controlling and managing.

| Requirement 1	Requirement 2	Requirement 3
Print quality control to avoid variation in printing process	Non-iterative method for generating DGCCs	A networked workflow

Automated CtP Calibration
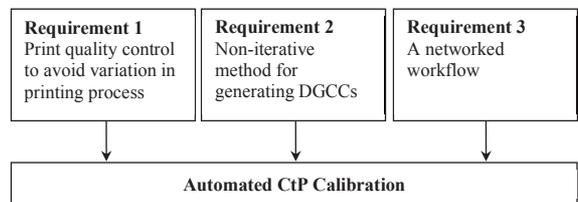
Figure 1: Three necessary requirements for Automated CtP Calibration

Figure 1 demonstrates these three necessary requirements for an automated CtP calibration system. These three necessary requirements are described in detail in the following three sub-sections.

2.1 Print quality control

A high number of parameters, such as consumables, the mechanical condition, maintenance and service of a printing machine, its setting and its adjustment by the operators, and temperature and humidity in the print room, influence the printing process and thereby the printed tone values. Offset printing is surely one of the most sensitive printing processes. Because of this fact the printing process should be controlled very often and carefully. An uncontrolled printing process is subject to relatively high variations.

Hence the first and a very important requirement for the automated CtP calibration workflow is the Print Quality Control (PQC). It includes the check of different target values in printing process and the check of different print quality criteria regarding the stability and reproducibility. Generating a DGCC and thereby a CtP calibration only makes sense in a stable and reproducible printing process. Therefore, for an automated CtP calibration system, a print quality control program is needed to check different print quality criteria before starting the calibration. Target ink value, tone values, maximum mid-tone spread, slurring, register variation and doubling (Hauck and Gooran, 2011a and 2015), and also ink trapping (Hauck and Gooran, 2011b and 2013) are the most important criteria that should be within the acceptable range and stable before and during the CtP calibration.

A print PQC-program suggested in this paper contains two separated modules. The first module of the PQC-program checks the print quality criteria according to ISO 12647-2:2013, and compares their values with a table containing the allowed tolerances for each print quality criterion. If during the production phase all values of the print quality criteria are within their acceptable range, then the program sends a message to the Work Control System (WCS). The WCS then sends a permission to generate a DGCC. If the print quality values are outside their acceptable range, the calibration procedure is interrupted, see Section 4 for more details. The second module of the PQC-program generates a DGCC using a non-iterative method.

2.2 Non-iterative dot gain compensation method

As known, the mathematical function characterizing dot gain is not linear and almost all existing methods for generating a DGCC for offset printing process are iterative (Hauck, 2013). This means that the generation

of DGCC is in action in a loop until the printed tone values are within the ISO 12647-2:2013 tolerance range. As mentioned earlier in this section, an iterative method for generating a DGCC cannot be used in this system. The second requirement for an automated CtP calibration workflow is therefore a non-iterative method for generating a DGCC (Hauck, 2012).

2.2.1 Measuring devices

Printing companies employ densitometer(s) and/or spectrometer(s) to control the printing process. For both densitometry and spectrometry there are two types of instruments. The first type only measures a spot. The other type called scanning densitometer or scanning spectrometer measures a number of spots which together build a bar like a print control bar. Figure 2 shows these two different layouts needed for an automated CtP calibration workflow. Figure 2(a) shows a standard layout with a print control bar only and Figure 2(b) shows the same layout with a print control bar in (1) and an additional bar (2) in Figure 2, to be used to measure the printed tone values.
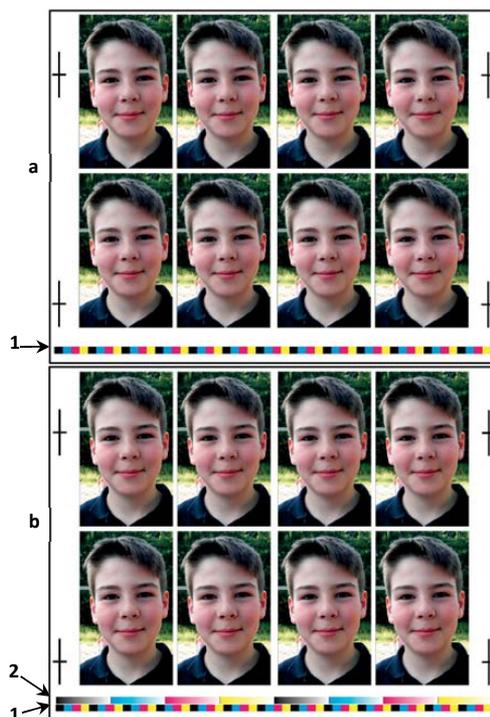
*Figure 2: (a) standard layout with the print control bar (marked 1), (b) the same layout with the second bar for measuring the printed tone values (marked 2)*

Scanning densitometers or scanning spectrometers are just the notation of such an instrument that is able to measure color bars and is not the same as scanners used in image capturing. Online and inline measuring devices are commonly used in the graphic industry

for industrial and economical printing processes. The additional bar shown in Figure 2(b) is needed for generating a DGCC in the proposed automated CtP calibration system. Hence the workflow with an automated CtP calibration system also needs a scanning spectrometer (online or inline). While for an online scan-spectrometer the operator has to take the sheets from the machine to the measuring device to be measured, in an inline scan-spectrometer the printed sheets are measured automatically in the machine during the printing production. However, an automated CtP calibration system can employ both types (online or inline) of spectrometers. It is however important that the measuring instrument can automatically scan a color bar. For example, the online scan-spectrometer ColorPilot (manroland) is able to scan two stacked color bars, see Figure 2(b). This scanning spectrometer was successfully tested for this purpose. However, any other online spectrometer that is able to scan two stacked color bars can be used as well. Another advanced print quality measuring device is proposed in Gugler and Hauck (2012).

2.2.2 Imposition program and templates

Imposition programs, for example Heidelberg Prinect Signa Station (Heidelberg, 2018a) or Kodak Preps (Kodak, 2018) are important programs for prepress, press, and post press. Normally, imposition defines the position of pages after folding a printing sheet for producing books. An imposition program might even be used in case there is no sheet folding, e.g. for packaging sheets or labeling sheets. An imposition program can employ different types of templates. A template contains a predefinition of the position of a print control bar, the register marks, and of course the reserved area for printing the layout of a job (Kipphan, 2001). In an imposition program it is possible to define the position of a printing control bar and all needed marks only once. Then all needed marks and the print control bar are set automatically by the imposition program. Hence for a standard print job without the generation of a DGCC the Template-I in Figure 3 is chosen as usual. For an automated CtP calibration at least two different templates are necessary for plate imaging. Figure 3 shows these two needed templates, where 1, 2, 3, and 4 show the print control bar, the tone value wedge (DGCC-bar), the reserved area for print layout and the register marks, respectively. Template-II in Figure 3 is needed if a DGCC has to be generated and therefore the DGCC-bar will be needed on the production sheets, more details in Section 4. Observe that Template-II contains all elements of Template-I plus a DGCC-bar. Hence in Template-II the size of the reserved area for print layout is 3–5 mm shorter in print direction than in Template-I. However this is no problem because the paper companies sell papers in standard

sizes, which mostly are 5 mm to 50 mm larger than the size of the print layouts. Exceptions are some packaging, label-printing and book-printing companies which use the entire surface of the paper.
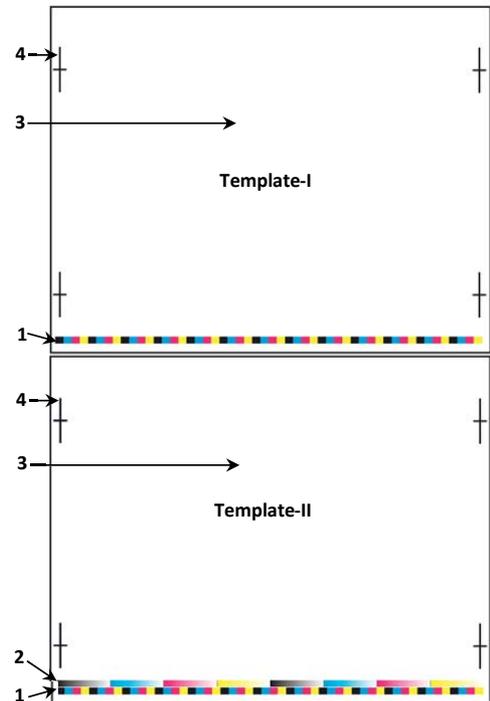
Figure 3: Template-I is the standard print template with one print control bar (1), Template-II has one additional bar, the stacked bar (2) which is the tone value wedge for generating a Dot Gain Compensation Curve

2.2.3 Dot Gain Compensation Curve Data Base

Most printing companies only use a small number of DGCCs (only one to five DGCCs). This is because of the complexity and the high cost of manually generating a DGCC and the fact that handling and managing more than five DGCCs without a WCS is practically impossible. Consequently, a big part of the print products cannot be printed with the completely correct TVI recommended by ISO 12647-2:2013.

As mentioned in Section 1, a huge number of DGCCs can be necessary in a printing workflow dependent on the number of combinations of consumables and printing workflows in a printing company. As will be demonstrated later in Figure 6(2), the DGCC Data Base (DGCC-DB) is a component of this automated CtP calibration system; DGCCs are saved and then loaded to be used dependent on the combination of consumables and printing workflows. The advantage of using DGCC-DB is that it is possible to save a large number of DGCCs. The managing (saving, overwriting, and calling) of the DGCCs in DGCC-DB has to be done via the WCS.

S. Hauck and S. Gooran – J. Print Media Technol. Res. 7(2018)3, 115–125

119

2.2.4 Renewal date for a Dot Gain Compensation Curve

A generated DGCC should be renewed after three to six months. The reason is that the quality of consumables and the print machine setting slightly change over the time and the climate in the printing room also changes in different seasons. These factors might cause a dot gain shift after a few months since the involved parameters were adjusted. Therefore, it is necessary to save the date of generating a DGCC and specify a date for the earliest (e.g. three months after the generation of the DGCC) and the latest (e.g. six months after generating the DGCC) renewal of DGCC. An already existing DGCC should be renewed between the earliest and the latest date. These dates are set in WCS as setting parameters. Figure 4 demonstrates the time bar of DGCC with three different points of time; namely the generation of a DGCC, the earliest date for renewing and the latest date for renewing a DGCC.
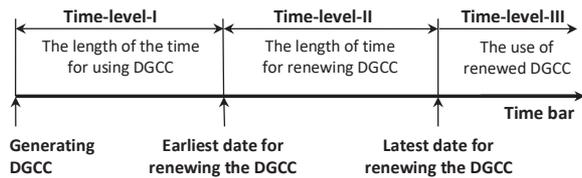

Figure 4: The time bar for generating, using, and renewing a Dot Gain Compensation Curve

These three points of time result in three different time corridors (Time-level-I to Time-level-III). A time-level is the time corridor (limit) between two points of time. For example, Time-level-I is the time corridor from generating a DGCC to its earliest time for renewal. The other time-levels have their own time corridor as shown in Figure 4.

2.2.5 Nomenclature of Dot Gain Compensation Curves

As mentioned before, in a printing company the number of necessary DGCCs depends on the number of combinations of consumables and print workflows, which can result in a high number of combinations. Hence for managing the DGCCs in the workflow it is necessary to have a distinct nomenclature for a generated DGCC. A useful DGCC-denotation should contain the information about the consumables, printing workflow and renewal date of a DGCC. Figure 5 demonstrates the coding of a DGCC nomenclature as an example in which part (a), the first number, demonstrates the used printing substrate group from the eight PSs according to ISO-12647-2:2013 description.
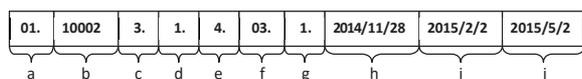

Figure 5: The nomenclature of a DGCC

In Figure 5, the five digits of part (b) specify the nomenclature of the used ink dependent on its color, fabrication and type. The next number in part (c) demonstrates the used printing plates dependent on their fabrication and types. Part (d) demonstrates the used blanket dependent on its fabrication and type. Part (e) demonstrates the dampening concentrates dependent on its fabrication and type. Part (f) demonstrates the printing machines (for example 03 in Figure 5 means the third printing machine in the print department). Part (g) demonstrates the print workflows (for example 1 for conventional printing, 2 for UV printing, 3 for alcohol reduced printing and so on). The dates in part (h) to (j) demonstrate the date of generating the DGCC, the earliest date for renewing the DGCC and the latest date for renewing the DGCC.

The demonstrated nomenclature can vary and be expanded dependent on the workflows in different printing companies. The WCS generates the numbers of nomenclature for a DGCC. The nomenclature of DGCC is saved together with DGCC in DGCC-DB. When a specific DGCC is needed, the WCS searches for it in the DGCC-DB using its nomenclature.

2.3 Networked workflow

The third requirement for an automated CtP calibration system is a networked workflow. Figure 6 shows the needed networked workflow for an automated CtP calibration system.

The demonstrated networked workflow contains the following components: (1) an extended Management Information System (MIS), or alternatively a WCS of printing machine manufacturer can also be used. In this paper, the term WCS is used for this module; (2) DGCC-DB, (3) RIP, (4) layout and print data, (5) imposition program with at least two different templates, (6) CtP, (7) printing plates, (8) printing machine, (9) press control desk with an integrated scan-online-spectrometer. The press control desk is the central part for controlling and commanding the printing machine. Item (10) is printed sheet to be measured and (11) PQC program including the non-iterative method for generating a DGCC. The (1), (2) and (11) are the novel parts in this workflow; all other parts are state of the art.

In such a networked workflow the WCS firstly checks if the needed DGCC already exists (see Section 3.1) in the DGCC-DB (Section 2.2.3). Therefore the WCS generates a list of consumables and the print workflow and builds a notation for needed DGCC (Section 2.2.5).

There are more scenarios possible to choose a DGCC which are explained in detail in Section 3.1.
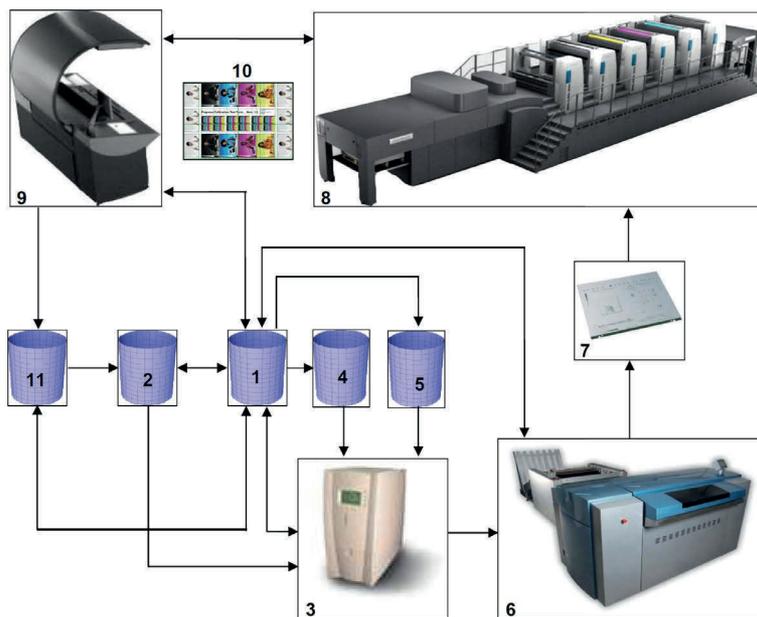
*Figure 6: The networked workflow for an automated CtP calibration: (1) extended MIS or alternatively a WCS,
(2) DGCC-DB, (3) RIP, (4) layout and print data, (5) imposition program, (6) CtP, (7) printing plates,
(8) printing machine, (9) press control desk, (10) printed sheet, (11) PQC program*
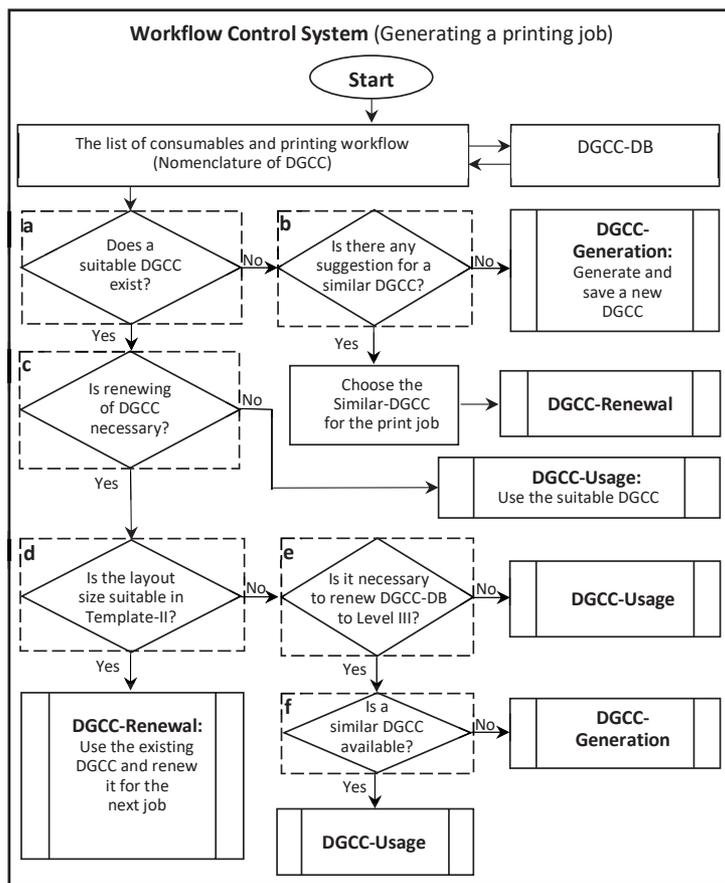
*Figure 7: Job generation in the WCS and choosing one of three possible choices
(DGCC-Generation, DGCC-Usage and DGCC-Renewal)*

S. Hauck and S. Gooran – J. Print Media Technol. Res. 7(2018)3, 115–125

121

3. Workflow Control System

For controlling a workflow with automated CtP calibration, a MIS can be used, but a better alternative is a WCS. The problem with some MIS is that an inconsistency between the systems and the components of a workflow still exists (Kühn und Grell, 2004). Because of this a WCS would work absolutely satisfactorily with prior matched workflow components (e.g. a specific RIP); WCS is the logical and neuronal head of a workflow. All communications and logical processes are controlled here. The needed commands and the order of operating and the definition of procedural hierarchy are managed by the controller. The WCS is best integrated in print machine manufacturers' network system or alternatively in a MIS. Examples for the network system of printing machine manufacturers are printnetwork system (manroland, 2018) developed by manroland and Prinect system (Heidelberg, 2018b) developed by Heidelberg.

In the printing workflow, if a job has to be printed with a suitable DGCC, the WCS first builds a list of demanded consumables and printing workflow and denote this list according to the nomenclature of DGCCs and searches for a DGCC or a similar DGCC in the DGCC-DB. There are therefore three possible scenarios:

1. DGCC-Generation: If in the DGCC-DB neither the DGCC nor a similar DGCC exists, a new DGCC has to be generated and saved in the DGCC-DB. This is explained in Section 4.1.

2. DGCC-Usage: If in the DGCC-DB the needed DGCC exists, then it can be used for the print production. This is explained in Section 4.2.

3. DGCC-Renewal: If in the DGCC-DB a DGCC at Time-level-III in Figure 4 or a similar DGCC exists, then it can be used for the print production but it has to be renewed during the print production. This is explained in Section 4.3.

After generating a job, the WCS has to decide on one of these three choices mentioned above in order to send the right DGCC to the RIP. The working principle of the WCS for this decision is demonstrated in Figure 7.

As mentioned before, the WCS makes a list of all needed consumables after generating a job. Then the information of this list is compared with the existing nomenclatures in DGCC-DB and then the decision in the step (a) is made (Figure 7).

If there is no suitable DGCC, then a similar DGCC (Section 4.3.1) is searched in the step (b), Figure 7. Depending on the result of decision (b) either the

DGCC-Renewal or the DGCC-Generation related to the job is carried out. In the decision (a), if a suitable DGCC is available, then the step (c) will be executed.

If the answer in the step (c) is "no" then the DGCC-Renewal related to the job generation of WCS and needed DGCC has to be activated. If the answer in the step (c) is "yes", then the decision in the step (d) has to be started. Now in order to generate a DGCC, Template-II has to be used. Hence the WCS checks if the reserved area is suitable for setting the print layout in Template-II (Section 2.2.2). If yes, then the DGCC-Renewal starts. Otherwise the decision in the step (e) is made to check whether the already found DGCC can still be used (Figure 4, Time-level-II). This results in the DGCC-Usage. Otherwise, if the DGCC is old and cannot be used (Figure 4, Time-level-III), the decision in the step (f) has to be executed. For this decision the WCS has to check if a similar DGCC is available or not. If a similar DGCC is available, then the DGCC-Usage, otherwise the DGCC-Generation will be performed.

4. Generating, using or renewing a Dot Gain Compensation Curve

As explained in Section 3, dependent on the needed consumables, printing workflow and the availability of a DGCC, the WCS decides on one of three choices: generating, using, or renewing a DGCC, as demonstrated in Figure 7. In this section, all these three possible choices and the corresponding processes are described.

4.1 Dot Gain Compensation Curve Generation

As discussed in Section 3.1, at the beginning of managing a printing job the WCS searches for an existing or similar DGCC in DGCC-DB dependent on consumable and workflow list. If there is no existing or similar DGCC or the existing or similar DGCC is in Time-level-III, the WCS will order the DGCC-Generation. A short time after using the system in the production, the generating procedure occurs less frequently compared to the DGCC-Usage or DGCC-Renewal. Figure 8 demonstrates the flowchart for the DGCC-Generation, i.e. the generation of a new DGCC and its saving in the DGCC-DB. If the WCS decides for the DGCC-Generation, then the imposition program will receive an order to use Template-II (Figure 3). After the halftoning and plate making through CtP, the printing can start. When the make-ready is finished, the production phase can start. In the very beginning of starting the system, there is still no DGCC available, and hence a printing test is needed for generating an initial DGCC before the production phase. For an exact generation of the DGCCs the printing process should be reproducible and the process variation (like target value variation, tone

value variation or register variation) should be within the tolerance ranges (Figure 1, Requirement 1). Hence, before the DGCC can be calculated, the stability of the printing process has to be checked. The DGCC-bar has to contain the elements allowing to check the stability of the printing process (Hauck and Gooran, 2011a; 2011b; 2013; 2015). In case of variation, the calibration process is to be interrupted and optimized. After the make-ready and stabilization of the printing process the DGCC-bar is measured for the evaluation and calculation of the DGCC. This workflow works economically, if the printing process is controlled and stable. During the production the operator of the printing machine has to take several printing sheets and measure them for controlling the printing machine and the inks. An inline spectrometer does this procedure automatically. If the variation in the printing process is within the tolerance range, then the measuring system will get permission to measure the DGCC-bar.

It is also possible to measure several printed sheets (commonly 5 to 10) to build an average value. For the calculation of DGCC in this automated workflow a non-iterative DGCC generating method is absolutely necessary (Figure 1, Requirement 2). The generated DGCC is saved in the DGCC-DB after generating a meaningful nomenclature. After having saved the new DGCC the WCS gets a feedback that the DGCC is saved, and the process will then successfully terminate.

4.2 Dot Gain Compensation Curve Usage

As discussed in Section 4.1, in the case of DGCC-Usage a DGCC can be used without the need to be renewed (Figure 4, Time-level-I). The WCS decides to use an existing DGCC and does not generate a new one. Figure 9 demonstrates the flowchart for the DGCC-Usage. For the DGCC-Usage, the imposition program receives an order from the WCS to use Template-I, see Figure 3(a).
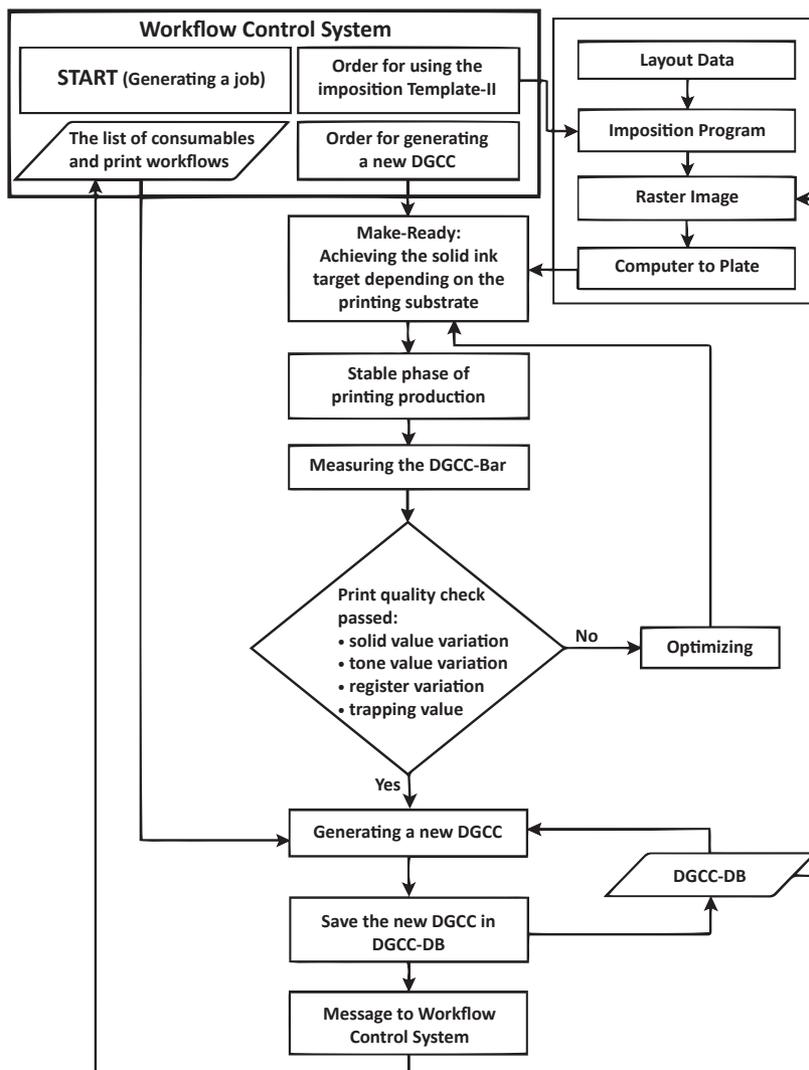

*Figure 8: Generating and saving a new Dot Gain Compensation Curve*
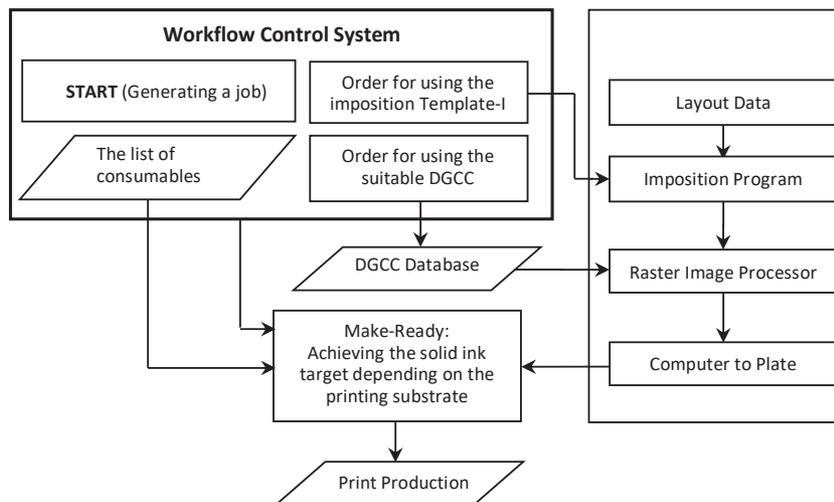
Figure 9: Using a suitable Dot Gain Compensation Curve

The WCS gives an order for the export of DGCC-Data from the DGCC-DB to the RIP. After the halftoning and plate making the make-ready at the printing machine can start. After the make-ready phase is finished, the printing production phase can start.

4.3 DGCC-Renewal

The WCS chooses the DGCC-Renewal if an existing DGCC is to be used for generating a new DGCC according to the used consumable and workflow in the printing production. The chosen DGCC can be an exactly needed DGCC according to the consumable and workflow list of WCS which is renewed (Figure 4, Time-level-II) or the chosen DGCC is just a similar DGCC. Hence in the latter case for the future need of an exact DGCC a new one has to be generated during the printing production. Figure 8 also demonstrates the flowchart for the DGCC-Renewal. The imposition program receives an order for using Template-II (Figure 3). The chosen DGCC is exported from DGCC-DB to the RIP. After the halftoning and plate making through the CtP the make-ready at the printing machine can start.

When the make-ready is finished, the printing production phase starts. As mentioned before, for an exact generation of the DGCC, the printing process has to be checked to make sure that the printing process variation is within the tolerance range. If this requirement is fulfilled, then the measuring system can measure the DGCC-bar.

Similar to the DGCC-Generation the non-iterative method calculates a new DGCC. After generating the new DGCC it is saved in DGCC-DB. For the Time-level-II (as demonstrated in Figure 4) the new DGCC replaces the old one in DGCC-DB. The WCS then gets a feedback that the process was successfully terminated.

4.3.1 Using Similar Dot Gain Compensation Curve

There are different priorities for the list of the used consumables and processes. For example, the most important priority for a DGCC is the group of printing substrates and the fabrication of the inks. Surely the type of the blanket or plate is also important, but not as important as the paper class and the fabrication of the ink. Dependent on the workflow and production, some consumables in the workflow can play a very important or a less important role in the printed tone values. This is important for searching for a similar DGCC in DGCC-DB if an available DGCC does not exist. The use of a similar DGCC reduces the number of the first choice of WCS for defining a print job (if in the DGCC-DB neither the DGCC nor a similar DGCC exists, a new DGCC is generated and saved in the DGCC-DB).

To clarify how to find a similar DGCC in DGCC-DB, an example is given. Assume that for a workflow manager the type of the substrate and the ink properties are the most important parameters. When searching for a DGCC in the DGCC-DB, the WCS checks if there is a DGCC generated using the same type of paper and ink. If so, then it checks for other parameters, such as plate. If, for example, the plate is not the same for this existing DGCC, it can still be considered to be a similar DGCC, because the plate is not of the higher priority.

5. Summary and discussion

To realize an automated CtP calibration workflow three requirements have to be fulfilled. The requirements are the controlling of print quality in order to avoid variation in the printing process, the non-iterative generation of DGCCs and the networked workflow. The first two requirements are realized and successfully applied.

The most parts of the third requirement are also state of the art, and only the WCS is to be developed. Hence this system is still not available. This paper described the needed control and the necessary logical communication between the workflow of the prepress and press.

There are three possible choices for a WCS in order to use a DGCC at the beginning of job definitions. These three choices are generating a new DGCC, using an available DGCC, and the combination of using and generating a DGCC (for example the renewal of a DGCC).

The suggested workflow allows to considerably reduce the costs and the time needed for generating or renewing the DGCCs. This system is useful for all printing companies which want to produce predictably, reproducibly and thus economically. The proposed automated CtP calibration workflow will facilitate a printing workflow with most productions following ISO-12647-2:2013 standard which will further increase the print quality. Furthermore, an automated CtP calibration workflow enormously reduces the work of the staff at the prepress, press, and quality management. It saves time and costs.

References

Gu, H., 2008, Character and Application of CTP Flow Calibration in System in Packing and Printing. *Packaging Engineering*, 2008(12), pp. 112–114.

Gugler, C. and Hauck, S., manroland AG. 2012. *Method for determining parameters relevant to the print quality of a printed product.* U.S. Pat. 8,089,667.

Hauck, S., Manroland Sheetfed GmbH. 2012. *Verfahren zum Bebildern von Druckbildträgern*. German Pat. DE 10 208 033 403 B4.

Hauck, S., Manroland Sheetfed GmbH. 2013. *Verfahren zum Bebildern von Druckbildträgern*. E.U. Pat. EP 2 349 718 B1.

Hauck, S. and Gooran, S., 2011a. An alternative method to determine register variation using spectrophotometry tool. In: *Proceedings of the TAGA 63rd Annual Technical Conference.* Pittsburgh, Pennsylvania, 6–9 March 2011. Sewickley: TAGA, pp. 46–47.

Hauck, S., and Gooran, S., 2011b. An alternative computational method of trapping for the printers at the press. In: *Proceedings of the TAGA 63rd Annual Technical Conference.* Pittsburgh, Pennsylvania, 6–9 March 2011. Sewickley: TAGA, pp. 51–52.

Hauck, S. and Gooran, S., 2013. Investigation of the effect of ink penetration and gloss on a proposed spectral trapping model for high quality glossy coated paper. *Journal of Print and Media Technology Research*, 2(4), pp. 235–244.

Hauck, S., and Gooran, S., 2015. A novel method to determine register variation of a press by a densitometry tool. *Journal of Print and Media Technology Research*, 4(2), pp. 95–102.

Heidelberg, 2018a. *Prinect Signa Station*. [online] Available at: <https://www.heidelberg.com/global/en/products/workflow/prinect_modules/production_management/prinect_prepress_manager_4/prinect_signa_station/prinect_signa_station.jsp> [Accessed 8 March 2018].

Heidelberg, 2018b. *Prinect Module.* [online] Available at: <https://www.heidelberg.com/global/de/lifecycle/workflow/prinect_modules/prinect_modules_overview/prinect_modules_overview.jsp> [Accessed 31 July 2018].

Hendersson, T.A, Eastman Kodak Company. 2013. *Providing calibration data for printer*. U.S. Pat. 8,564,861.

Homann, J.-P., 2007. *Digitales Colormanagement: Grundlagen und Strategien zur Druckproduktion mit ICC-Profilen, der ISO 12647-2 und PDF/X-1a*. 3. Aufl. Berlin, Heidelberg: Springer Verlag.

International Organization for Standardization, 2013. ISO 12647-2:2013 *Graphic technology – Process control for the production of halftone color separations, proof and production prints – Part 2: Offset lithographic processes*. Geneva: ISO.

Kipphan, H. ed., 2001. *Handbook of print media: technologies and production methods*. Berlin, Heidelberg: Springer Verlag, pp. 100–103; pp. 213–221; pp. 231–232; pp. 236–239; pp. 247–250.

Kodak, 2018. *The leading solution for automated, error-free impositions, version 7*. [online] Available at: <https://nmac.to/preps/> [Accessed 8 March 2018].

Koifman, I., Weiss, A. and Fisher, Y., Creo IL. Ltd. 2003. *Dot gain calibration method and apparatus.* E.U. Pat. EP 1 365 576 A2.

Kühn, W. and Grell, M., 2004. *JDF: Prozessintegration, Technologie, Produktdarstellung*. Berlin, Heidelberg: Springer-Verlag.

Leng, C.-f., 2009. Research on Characteristic Curve for CtP. *Packaging Engineering*, 2009(6), pp. 63–64.

manroland, 2018. *printnetwork*. [online] Available at: <http://www.manrolandsheetfed.com/en-GB/460/printnetwork-reg> [Accessed 8 March 2018].

McDowell, D.Q., 2007. Method for calibration of a printing system with digital data using near-neutral scales. In: *Proceedings of the TAGA 59th Annual Technical Conference.* Pittsburgh, Pennsylvania, 18–21 March 2007. Sewickley: TAGA, pp. 51–52.

Mittelhaus, M., 2000. *Computer to Plate – Die Herausforderung.* Voltlage, Germany: Michael Mittelhaus System + Beratung + Schulung.

Schmitt, U., Ondrusch, M. and Rauh, T., 2010. *Practice report: guidelines for the Fogra CtP acceptance test.* München: Fogra.

S. Hauck and S. Gooran – J. Print Media Technol. Res. 7(2018)3, 115–125

125

Abbreviations

CM	Color Management
CtP	Computer to Plate
DGCC	Dot Gain Compensation Curve
DGCC-DB	DGCC Data Base
ICC	International Color Consortium
MIS	Management Information System
PC	Print Conditions
PQC	Print Quality Control
PS	Print Substrate
RIP	Raster Image Processor
TVI	Tone Value Increase
WCS	Workflow Control System

Effect of printing parameters on microwave performance of printed chipless RFID tags

Sika Shrestha and Nemai Chandra Karmakar

Department of Electrical and Computer System Engineering,
Monash University, Australia

sika.shrestha@monash.edu
nemai.karmakar@monash.edu

Abstract

The chipless Radio Frequency Identification system (RFID) will revolutionize the identification market due to its low-cost tagging methods. The printed version of the chipless tag is able to reduce the cost to few cents per tag. The microwave performance of the printed chipless tag is suffered due to the practical limitations of the overall fabrication procedure through printing. The bandwidth broadening is unavoidable for the printed tag, which directly hits on the data capacity. Similarly, the strength of the microwave signal is also degraded for printed RFID tag, which affects the reading distance of the tag. The fabrication of chipless RFID tag via printing involves several parameters such as the conductive ink processing condition, the substrate parameters and the geometrical dimension of the printed tag. We need to understand the relationship between these printing parameters with the microwave response of the printed tag, to analyze the key parameters affecting the response of the printed tag. A comprehensive experimental investigation is performed in this paper to evaluate the relationship between the printing parameters and microwave response of the printed tag. The printing parameters include conductive ink sintering type and sintering conditions and deposited ink thickness. A high-speed photonic sintering process is adopted for the first time to sinter chipless RFID tag so that chipless RFID tag can be manufactured using fast roll-to-roll printing process. Optimum conditions for the photon-sintering process are deduced through experimental analysis for conductive inks of various viscosity. The effect of the geometrical dimensions of the printed strip and the printing accuracy is also analyzed to understand the limitations of the printing technique in terms of tag size. The issues seen in the printed RFID tag, their reason and the solution is then deduced in the final section so that the printed chipless tag can accommodate the real world limitations to make viable commercial outcome.

Keywords: RFID communication, screen-printing technology, conductive ink, oven sintering, photon sintering

1. Introduction

Chipped Radio Frequency Identification (RFID) system is not able to compete with ubiquitous barcode system and make a remarkable position in the market for automatic identification and data capture technology owing to its higher cost and non-planar nature of RFID tag. A minimum cost of five cents is achievable for chipped RFID tag, only in the case of mass production. The high volume customers such as Walmart uses several hundreds of millions of tags per year. However, the tag price of 5 cents to 10 cents is still too expensive for low-cost applications. The low price items with low-profit margins can only be tagged using the tag costing a fraction of a cent. Also, the structure of chip makes the RFID tag non-planar, which does not allow it to be used on commercial substrates such as banknotes and other paper documents. A new domain of RFID system which does not require the chip for data encoding in RFID tag is able to reduce the tag cost and make it planar. The removal of the chip in the chipless tag has made it planar and provided an opportunity for obtaining a fully functional printed RFID tag for many low-cost applications. This chipless RFID tag can act as RF barcodes if they are printed on flexible substrates and on commercial items like a barcode. The tag cost can be significantly lowered through manufacturing of chipless tag using an additive, high-throughput printing process, and low-cost conductive inks. It has been predicted by Das and Harrop (2010) that 624 billion chipless tags will be sold in 2019 if the targeted low cost is achieved.

The data encoding in a chipless RFID system is based on the electromagnetic signature since there is no chip

or memory to store the tag identification data (tag ID). The identification data generated by the chipless tag can be based on frequency signature (Preradovic and Karmakar, 2009; Khan, Tahir, and Cheema, 2016; Noor, et al., 2016; Sajitha, et al., 2016; Huang and Su, 2017), time domain reflectometry (Chamarti and Varahramyan, 2006; Forouzandeh and Karmakar, 2015; Mandel, et al., 2015), image domain (Zomorrodi, 2015), and phase domain (Balbin and Karmakar, 2009; Genovesi, et al., 2014; 2016). The frequency signature based chipless RFID tags are multi-resonator tags, where each resonator encodes 1 bit. The presence of resonance in predetermined frequency is identified as a data bit. The resonator exhibits the frequency selective behaviour and abrupt spectral features in amplitude spectrum are used to encode digital data bits. The chipless RFID tags based on time domain reflectometry identify the tag ID in the form of the delay in the train of echoes to an interrogation signal sent by the reader. The presence and absence of resonator in the tag are identified using the unique electromagnetic (EM) image in image domain based chipless RFID tag. The abrupt spectral features in the phase spectrum exhibited by the resonator are considered as the tag ID for data encoding based on phase domain.

Various printed chipless RFID tags have been reported in the literature (Vena, et al., 2013; 2014; Borgese, et al., 2017; Jeon, et al., 2017; Herrojo, et al., 2018) but the issues seen in printed tag response during the fabrication of chipless RFID tag via printing are not explored in detail. To understand the issues with the response from the printed tag, the relationship between the various parameters involved in the printing process and the microwave response needs to be analyzed. In this paper, chipless RFID tag generating the tag ID in the frequency domain is printed using screen-printing technology. The microwave response of the printed tag is analyzed to investigate the effect of various printing parameters on the performance of chipless RFID tag.

The printing of chipless RFID tags involves two main steps: printing and sintering (annealing). The printing is performed using a commercial printing technique such as screen-printing and ink-jet printing using conductive ink. The metal paste or liquid metal which are mixed with binders that help the ink to remain attached to the substrate surface are used as conductive inks for printing of chipless tags. The solid content of silver in these inks is not 100 per cent so they have low conductivity compared to relatively pure metals like copper or aluminium.

The parameters involved in the fabrication of printed RFID tag are shown in Figure 1. The paper is organised as per this figure. The deposited ink thickness can get varied during different printing procedures and the

effect of varying deposited ink thickness and optimum required thickness is analyzed in Section 2. The sintering process removes the resistive elements, forming the conductive path. The sintering of the printed sample is performed using oven sintering in Section 3. A high-speed photonic sintering process is applied on the printed tags in Section 4 to make the manufacturing of tags through printing, adaptable to the industrial roll-to-toll printing process. The effect of the ink processing conditions for various inks is examined for oven-sintered and photon-sintered printed tags in these sections. The effect of tag dimension on electrical parameters of the printed strip is shown in Section 5. The inaccuracy seen in printed dimensions is depicted in Section 7 with a possible solution. Finally, a dependency chart between the printed tag response and the printing parameters is explained in Section 8, which will assist in figuring out the bottleneck in obtaining a high fidelity printed tag response and assess the alteration required in the tag and the manufacturing process to enhance the printed tag response.
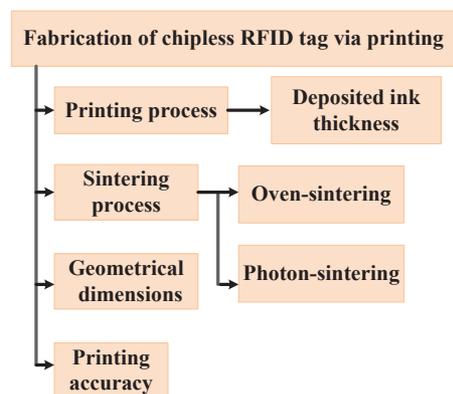
Figure 1: Various printing parameters affecting the microwave performance of printed chipless RFID tag

2. Effect of ink thickness on microwave performance of the printed tag

The conductor thickness of the printed tags is usually lower than the thickness of copper metallization in the Printed Circuit Board (PCB) fabricated tag. The thickness of ink deposited in printing process mainly depends on the printing technique and ink viscosity. The signal loss occurs when the deposited ink thickness is less than the skin depth at the operating frequency. This is because of the leakage of the microwave signal through the dielectric substrate layer for low conductive ink thickness which results in signal penetration loss as it propagates along the conducting guiding structure. The consequence is the spread of the quality factor of the resonator with strong negative impact on the data capacity of the resonator. In this section, the effect of ink thickness on the microwave performance

of printed tags has been analyzed and an approximate minimum thickness required to obtain acceptable microwave performance is evaluated. Initially, the rectangular bars of 2 mm width are printed using silver-based conductive ink named 'SHR-2'. The details of 'SHR-2' ink are given in Table 1 (note: 1 mil = 25.4 µm). The sample is printed on polyethylene terephthalate (PET) substrate which can withstand up to 250 °C. The sheet resistance of the printed strip is measured using a four-point probe SRM-232. The sheet resistance of rectangular printed strips obtained for varying ink thickness is plotted in Figure 2. Five sheet resistance and five thickness values are averaged for sheet resistance and thickness values respectively in this section and all other following sections. The sheet resistance is inversely proportional to the deposited ink thickness. The resistance is low for higher thickness as the amount of conductive material is less for low thickness.

Table 1: Details of experimented conductive inks

| Ink name	Metal content	Sintering conditions	Sheet resistance (Ω/sq/mil)
SHR-2	68.5 %	120 °C for 15 min	<0.010
SHR-1	84.0 %	110 °C for 5 min	<0.010
SHR-5	76.0 %	150 °C for 5 min	<0.005
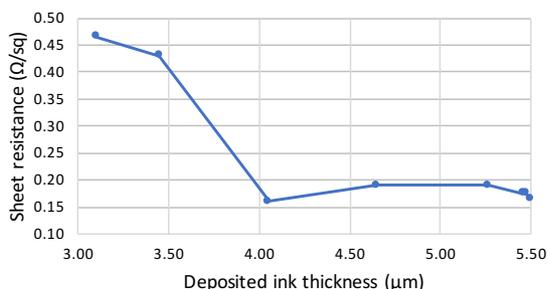
Figure 2: Sheet resistance for different deposited ink thicknesses (for a rectangular bar of width 2 mm, printed using 'SHR-2' ink on PET substrate, sintered at 120 °C for 15 min)

The modified version of Electric-LC (ELC) resonator (Naqui, et al., 2014) is considered as chipless RFID tag in this paper. The RFID tags printed using 'SHR-2' screen-printing ink on PET substrate tend to have different thickness because of manual screen printing. The thickness varied from 1 µm to 8 µm. The tag with at least 3 µm thickness gave detectable microwave response. The microwave performance of the chipless RFID printed tag can be evaluated in terms of 3 dB bandwidth and Radar Cross Section (RCS) amplitude as shown in Figure 3. The bandwidth is obtained as the frequency range that lies within 3 dB of the response at its peak. The electromagnetic response reflected from the tag is considered as the identification data in

the chipless RFID system and the reflected response is obtained in terms of RCS. The RCS amplitude is the strength of the received signal, which is the difference between the peak and null of the signal as shown in Figure 3.
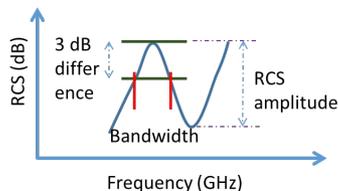

Figure 3: Illustration of bandwidth and radar cross section amplitude difference

The RCS amplitude and 3 dB bandwidth are obtained for the first resonant frequency (3.9 GHz) of the printed tags in this section and all following sections. In frequency coded chipless RFID tags, the bandwidth of the electromagnetic response needs to be low so that higher amount of data bits can get fitted within the given frequency range.

The higher value of RCS amplitude, which is the strength of the signal, increases the reading distance of the tag. The measured 3 dB bandwidth and RCS amplitude for varying ink thicknesses are depicted in Figure 4. The bandwidth is broadened for the chipless RFID tags compared to fabricated tag because of low conductivity of the ink. The bandwidth broadening is reduced for higher resonator thickness. The strength of the signal or the RCS amplitude has also risen for higher deposition of conductive ink. If we considered 250 MHz as the acceptable bandwidth for experimented tags in this section, then, the thickness of the resonator needs to be at least 6 µm.
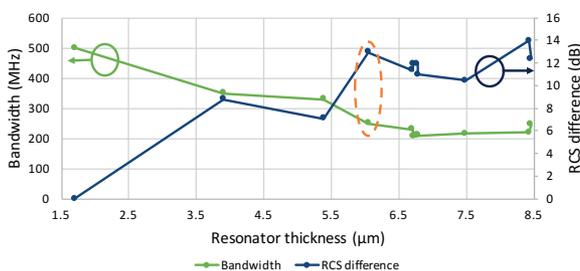
Figure 4: Microwave performance of RFID tags printed using 'SHR-2' ink for different deposited ink thicknesses

To understand the relation of the skin effect with the thickness of deposited ink, the skin depth is calculated for the frequency range from 4 GHz to 8 GHz for three different conductivity values and is shown in Figure 5. The conductivity obtained for this print is $1.8 \cdot 10^6$ S/m. The previous analysis shows that 6 µm are the minimum thickness required at 3.9 GHz. Figure 5 shows that at 3.9 GHz, the skin depth is around 6 µm. Hence,

the thickness of the deposited ink should be at least around the skin depth at the given frequency.
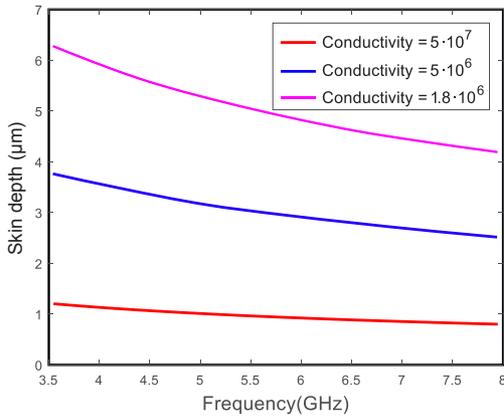
Figure 5: Skin depth versus frequency (3.5–8.0 GHz)

Therefore, the higher thickness of deposited conductive ink is desirable to obtain a response with low resistance, less bandwidth broadening, and higher RCS amplitude. The screen-printing technique is able to provide higher ink thickness compared to other printing techniques. A multiple passes of printing can be employed in other printing techniques such as ink-jet printing and gravure printing to increase the ink thickness.

3. Oven sintering of printed RFID tag

The microwave response of the chipless RFID tag, when printed using conductive ink, is highly dependent on the processing conditions of the ink. The conductive ink contains a resistive element such as dispersant material along with conductive metal pigment. The metal particles in the ink are surrounded by the dispersant material which keep the particles apart from each other and electrical conductivity does not form (Halonen, et al., 2013). These ink dispersants need to be removed in order to connect the conductive particles to form functional ink strips. The ink is passed through a heating process known as sintering to disorder/melt/ evaporate the dispersant and other resistive solvents to form the conductive paths. The sintering process also promotes the formation and coalescence of printed conductive features, which improves the electrical conductivity and the mechanical adhesion (Lukacs, Pietriková, and Cabuk, 2017). This section investigates the relationship between the ink processing parameters and the microwave performance of the printed tags for oven-sintered samples.

The oven sintering process is strongly connected with the conditions of technological process temperature and time (Lukacs, Pietriková and Cabuk, 2017).

The screen-printed rectangular bar using 'SHR-2' ink and having 2 mm width was sintered at four different conditions. The sheet resistance and thickness were measured using the four-point probe (SRM-232) and optical profiler (Bruker contour GT-K), respectively, and the conductivity is calculated using Equation [1]

$$\sigma = \frac{1}{R_s \cdot t} \qquad [1]$$

where σ is the conductivity, R_s is the sheet resistance and t is the thickness of deposited ink. Figure 6 shows the sheet resistance and conductivity of the printed bars.

The sheet resistance was significantly reduced from 0.4 Ω/sq to 0.1 Ω/sq when the sintering temperature increased from 80 °C to 120 °C and hence the conductivity increment is also noteworthy. The higher sintering temperature removes the higher amount of resistive component allowing more metal component to form a conductive path which thus increases the conductivity. The longer sintering time only brought a slight increment in the conductivity as seen for samples sintered at 80 °C/10 min and 80 °C/30 min. Hence, the sintering temperature plays a contributing role rather than sintering time to increase the conductivity of printed strips.
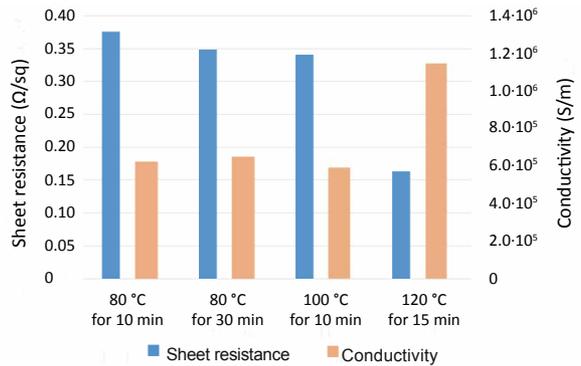
Figure 6: Conductivity obtained for printed strips sintered at different temperature of samples printed using 'SHR-2'

The microwave performance of the printed chipless RFID tags was investigated in terms of RCS amplitude and 3 dB bandwidth (Figure 3) for varying ink processing conditions. The RCS amplitude and bandwidth of samples printed using 'SHR-2' ink and sintered at different temperatures is depicted in Figure 7. Since the conductivity of the ink is increased for higher sintering temperature, the bandwidth of the first peak is also decreased up to 212 MHz. The bandwidth broadening is unavoidable because of low conductivity of the ink. However, we can minimize the bandwidth broadening through the sintering of ink at a higher temperature. The strength of resonance is also improved for higher sintering temperature.
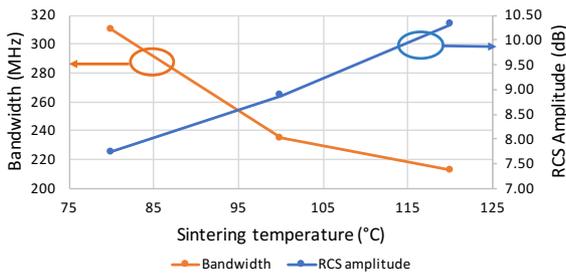
Figure 7: Microwave performance of RFID tags printed using 'SHR-2' ink for different sintering temperatures

The effect of sintering temperature on microwave performance of RFID tags printed using different inks is also investigated in Figure 8.

The higher sintering temperature of the conductive ink does not guarantee the enhanced microwave performance of the printed RFID tag. It also depends on the ink composition and formulation of the conductive ink procured from the ink supplier. Another ink supplier whose ink is named 'SHR-1' has stated its metal content as 84 % and recommended sintering temperature as 110 °C/5 min. The metal content for 'SHR-2' ink is 68.5 % and recommended processing temperature is 120 °C/15 min as per the ink supplier. However, the tag printed using 'SHR-2' ink, sintered at 80 °C has higher RCS amplitude and lower bandwidth compared to tag printed using 'SHR-1' ink, sintered at 100 °C. The third conductive ink, 'SHR-5' ink sintered at its recommended conditions (150 °C/10 min) is able to lessen the bandwidth up to 170 MHz and increase the RCS amplitude to 12 dB. The higher metal content gives better conductivity and hence better RF performance. The details of the experimented inks are shown in Table 1. The amount of metal content claimed by the supplier of 'SHR-1' ink may not be accurate as 'SHR-2' ink is able to give better performance. The simulated bandwidth of the exper-

imented chipless RFID tag having bulk copper as its metallization for its peak at 3.9 GHz is 70 MHz. Hence, among the experimented ink, the minimum bandwidth broadening of 100 MHz is seen for 'SHR-5' ink.

A simulation was performed to evaluate the relationship between the conductivity and bandwidth of the experimented chipless RFID resonators. The simulated bandwidth of the chipless RFID resonators obtained for various conductivities is shown in Figure 9. The bandwidth of the resonator is inversely proportional to the conductivity of the printed track. For higher conductivity, the bandwidth is low.
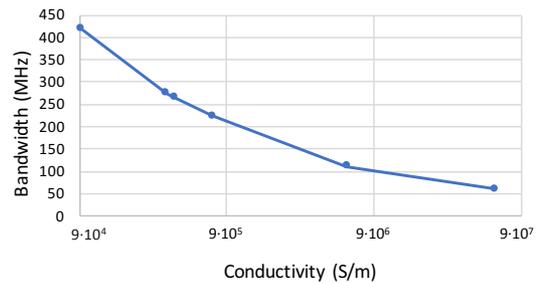
Figure 9: Simulated conductivity versus bandwidth

This means that the higher sintering temperature resulted in higher conductivity of ink and consequently, the printed tag is able to have less bandwidth broadening and better signal strength. The ink formulation in terms of metal content played a significant role in increasing the ink conductivity.

4. Photon sintering of printed RFID tags

The high volume manufacture of printed chipless RFID tags by any roll-to-roll printing process should satisfy specific industry standards. The production of the low-cost printed tag includes conductive ink printing and
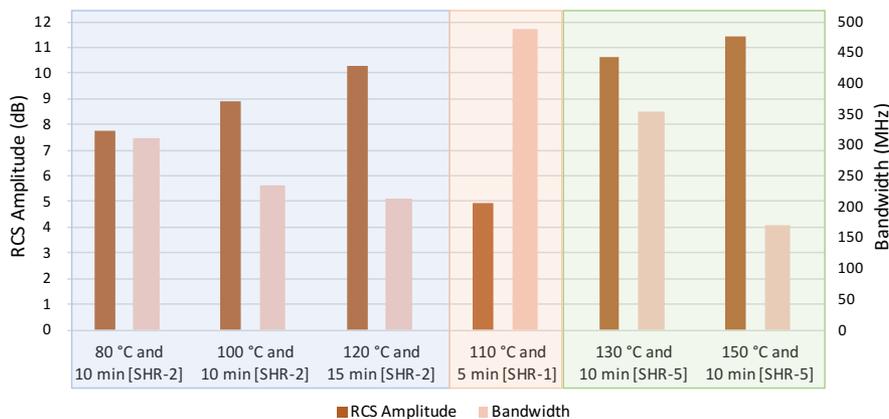
Figure 8: Microwave performance of circular ELC tag printed using 'SHR-2', 'SHR-1', and 'SHR-5' ink for different sintering temperatures

sintering process. The tags printed in the previous section were sintered using oven sintering process which requires few minutes to generate sufficient conductivity to obtain a workable printed tag. However, during the industrial manufacturing process, the sintering needs to be completed in a few seconds so that it can be suited for the roll-to-roll process. Also, most of the commercial substrates may not be able to withstand the higher temperature sintering requirement. So, a sintering process which can sinter at high temperature without altering the substrate physical properties is essential. Hence, a photonic sintering process which requires only a fraction of seconds for sintering is elucidated in this section. Optimum photon sintering conditions to obtain maximum ink conductivity is deduced after the analysis of the relation between the ink processing parameters and the electrical properties of the sintered samples.

Photonic sintering is the sintering of the printed track using high energy short pulse of light from a flash lamp. Using this technology, it is possible to attain a significantly higher temperature than the substrate can withstand in oven sintering process. In Schroder (2011), it is claimed that PET which normally has a maximum working temperature of 150 °C, can be processed at 1 000 °C using photonic curing system. The pulse of light is so fast that the back side of the substrate is not heated significantly during the pulse.

The printed samples were photon-sintered using Xenon S-2100a (XENON Corporation, 2010). The S-2100a has selectable pulse duration from 100 µs to 2 000 µs and adjustable pulse energy from 100 J to 2 000 J. The lamp voltage can range from 1.6 kV to 3.0 kV with digital control. The initial photon sintering is performed on rectangular printed bars. The printed bars when sintered with the same pulse width, at the same distance gave low resistance for high voltage as seen in Table 2.

Table 2: Sheet resistivity of printed bars, photon-sintered at different voltages

Voltage (kV)	Distance (inch)	Pulse width (µs)	Sheet resistivity (Ω/sq)
3	0.125	2 000	1.913
2	0.125	2 000	3.633

Then, the photon sintering is performed by placing the printed tracks at varying distance from the lamp. The distance of the sample has a significant effect on the amount of light absorbed by the sample. For instance, there will be a 60 % decrease in the energy when the sample is positioned 3 inches away from the lamp rather than 1 inch. The obtained sheet resistivity of printed bars with 400 µm width for varying distance of the sample from the lamp is shown in Figure 10. The

distance has a linear relationship with the sheet resistance as decreasing the distance between the lamp and the sample increases the energy with which the sample is sintered as shown in Figure 10. The 9.75 inch is the shortest distance between the flash lamp and the sample and hence has the lowest sheet resistance.
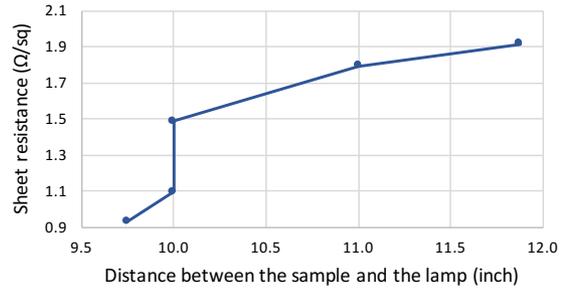
Figure 10: Sheet resistivity of printed tracks of 400 µm width photon-sintered at varying distance from the flash lamp

4.1 Photon sintering of chipless RFID tags printed on PET substrate

The resistance is low for higher voltage and samples near to the flash lamp, as discussed in the previous section. However, it is not practically feasible to place the sample so close to the flash lamp (9.75 inches). If ink sputtering occurs during the sintering process, then it can damage the lamps. In this section, the photon sintering of rectangular bars and chipless RFID tags is performed using covering material to avoid the sputtering of ink. The voltage is kept constant at the highest voltage (3 kV) and longest pulse width (2 000 µs) is used in sintering of all samples. The distance between the sample and the lamp is varied to find the best height of the sample so that the sample can receive uniform sintering without getting burnt.

Table 3 shows the summary of the photon sintering performed on PET substrate printed using 'SHR-2' ink. The Images 1 to 6 in Table 3 for sintered samples were captured using a digital microscope Dynolite (2.0 MP) with the 10 × magnification. In this section, the single-sided and two-sided photon sintering is performed. The use of quartz covering burnt the sample (it changed into grey colour and ink bubbles were seen initially but later ink came off). The two-sided sintering with samples covered by quartz, which involves sintering from both ink side and the substrate side, is also not able to protect the sample from getting damaged. Hence, the use of quartz covering generated excessive heat during the photon sintering of the silver printed track.

When the covering lid was changed to Pyrex for the same setting, the sample was not sintered properly but bubbles were seen at the edge of the bar as seen

Table 3: Photon-sintering of printed samples using 'SHR-2' ink with voltage of 3 kV

Distance (inch)	Sintered side (Covering)	Sheet resistance (Ω/sq)	Comment	Images from Dynolite
10.0	Ink side (Quartz)	–	Sample get burnt	Image 1: Rectangular bar 'a'
10.5	Substrate side – 1st Ink side – 2nd (Quartz)	–	Non-uniform sintering and sample was damaged	Image 2: Rectangular bar 'g'
10.0	Ink side (Pyrex)	0.287	Sheet resistance is less but visually the ununiform sintering was seen	Image 3: Rectangular bar 'b'
11.0	Ink side (Pyrex)	0.438	RF signals present for a tag with a bandwidth of 380 MHz	– **'A'**
10.5	Ink side (Pyrex)	0.349	RF signals present for a tag with a bandwidth of 285 MHz	**'B'** Image 4: Rectangular bar 'k'
10.5	Ink side – 1st Substrate side – 2nd (Pyrex)	0.315	Visually the non-uniform sintering was seen	Image 5: Rectangular bar 'i'
10.5	Substrate side – 1st Ink side – 2nd (Pyrex)	0.326	Visually the non-uniform sintering was seen	Image 6: Rectangular bar 'h'
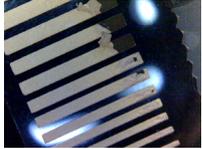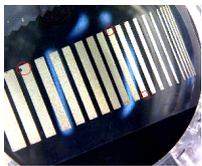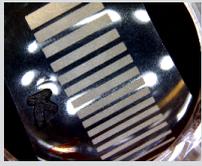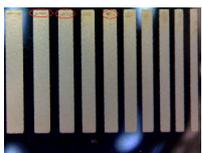
for rectangular bar (Image 3, in Table 3). The distance of 11 inches and 10.5 inches from the lamp gave uniform sintering. The sintering at two sides (ink side and film side) using Pyrex resulted in bubbles (Images 5 and 6, in Table 3) even though sheet resistance was less compared to other photon-sintered sample. Thus, the experimental investigation shows that the voltage of 3 kV, a distance of 10.5 inches, the pulse width of 2000 μs, Pyrex covering and one-sided photon sintering are the optimum conditions for the printed chipless tag on PET substrate

as they gave uniform sintering and low resistance compared to other samples. The microwave performance was measured for the tags that are coloured grey in Table 3. Let us consider the sample placed at 11.0 inches and 10.5 inches as 'A' and 'B', respectively. Table 4 shows the measured bandwidth and RCS difference for the measured photon-sintered tags with their corresponding sample names. Hence a detectable electromagnetic response is obtained for printed RFID tags sintered using the photon sintering process on PET substrate.

Table 4: Radar cross section and bandwidth of photon-sintered tags

Sample name	Thickness (μm)	Sheet resistance (Ω/sq)	Conductivity (S/m)	Bandwidth (MHz)	RCS (dB)
'B'	6.626	0.349	$4.32 \cdot 10^5$	285	9.51
'A'	5.696	0.438	$4.01 \cdot 10^5$	380	6.79

4.2 Comparison of photon-sintered and oven-sintered samples

The RFID tags sintered using oven and photon sintering can have variation in their conductivity and microwave performance. The sheet resistance, conductivity and mean roughness of samples printed using 'SHR-2' ink on PET substrate and sintered using the oven and photon sintering process is shown in Table 5. The photon sintering is performed with the optimum settings as explained in Section 4.1. The sintering process evaporates the dispersion solvent and sinters the left metallic particles to form conductive lines. The oven sintering process since it takes longer time is able to produce low resistance conductive line compared to photon sintering process. However, the sheet resistance is only increased by 0.3 Ω/sq when the samples are sintered

using photon sintering. The conductivity is correspondingly higher for oven sintering. The mean roughness of the printed tracks is measured using Bruker contour GT-K optical profiler. The mean roughness of rectangular bars and RFID tags is also compared in Table 5 for both sintering processes and it is seen that the roughness of the printed samples is not significantly affected by the change in sintering procedure. The microwave performance in terms of 3 dB bandwidth and RCS amplitude for tags sintered using box-oven and photon sintering is shown in Figure 11. The photon sintering of the tag performed with the samples placed at a 10.5 inch distance from the flash lamp is comparable to the oven-sintered tag at 80 °C for 10 minutes as this photon-sintered tag has rather low bandwidth and high RCS strength. The oven-sintered tag at 120 °C for 10 minutes has the best microwave response but these

Table 5: Sheet resistance, conductivity and mean roughness of oven-sintered and photon-sintered samples

| Sintering process	Sheet resistance (Ω/sq)	Thickness (μm)	Conductivity (S/m)	Mean roughness (μm)
Photon sintering	0.3490	6.402	$4.48 \cdot 10^5$	1.310
	0.4380	4.300	$5.31 \cdot 10^5$	1.115
	0.4040	5.492	$4.51 \cdot 10^5$	1.184
Oven sintering (120 °C/10 min)	0.1662	5.494	$1.10 \cdot 10^5$	1.228
	0.1880	4.906	$1.08 \cdot 10^5$	1.485
	0.1810	5.330	$1.04 \cdot 10^5$	1.360
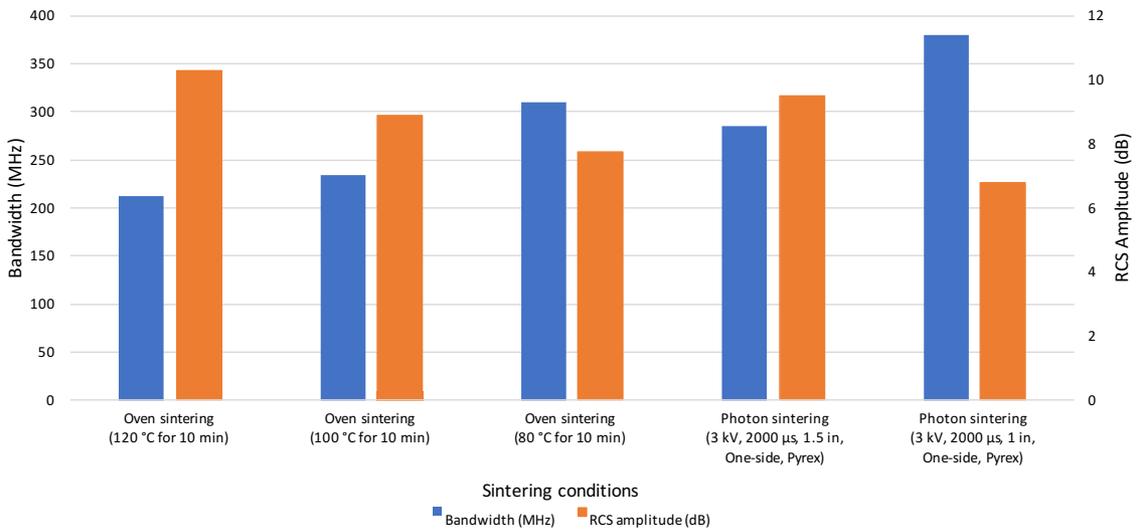
Figure 11: Microwave performance of oven-sintered and photon-sintered RFID tags (4 bit circular ELC tag printed using 'SHR-2' ink on PET substrate)

sintering conditions can be unsuitable for some commercial low-temperature substrates. The photon-sintered sample is able to obtain the lowest bandwidth of 285 MHz and the highest RCS amplitude of 9.51 which can be considered as a detectable tag ID.

4.3 Two-sided photon sintering of chipless RFID tag

In the previous section, the photon sintering is performed on a PET substrate for chipless RFID tags. The optimum settings were able to give the sheet resistance of 0.349 Ω/sq and a minimum bandwidth of 285 MHz with RCS amplitude of 9.51 dB. In this section, the photon sintering process is further optimized to obtain better RF performance and have the response comparable to the best result obtained from the oven sintering process. The photon sintering is performed on the more challenging substrate, biaxially oriented polypropylene (BOPP) polymerised with dicumyl peroxide (DCP), which cannot withstand the temperature higher than 80 °C. The issues seen in the previous section are samples getting burnt, with bubbles seen, which indicates the use of high power. Hence, to reduce the power exposed to the samples and to obtain uniform sintering, two-sided and two-times sintering has been utilized in this section. The two-sided sintering in

the previous section could not give a useful response because of high power, so in this section low voltage is tried to avoid non-uniform sintering.

In this section, the photon sintering is performed for inks with different viscosity to verify the versatility of photon sintering process. The photon sintering is performed on printed samples using three conductive inks: 'SHR-1', 'SHR-2', and 'SHR-4'. The viscosity of these inks and their wet ink layer thickness measured using Bruker contour GT-K optical profiler is shown in Table 6. The viscous ink deposits lower thickness compared to less viscous ink. The highest thickness was achieved with the ink 'SHR-4'.

Table 6: Thickness of printed samples for different inks

Ink name	Viscosity (Pa·s)	Sample description	Wet thickness (μm)
SHR-1	29.0	Not pre-dried sample	3.894
		Pre-dried sample	5.008
SHR-2	17.5	Not pre-dried sample	5.404
		Pre-dried sample	5.350
SHR-4	15.0	Not pre-dried sample	7.386
		Pre-dried sample	7.544

Table 7: Photon sintering of samples printed using 'SHR-2' ink on BOPP DCP substrate (distance = 1.5 inches from the lamp)

Sintering condition	No. of passes	Pulse width (μs)	Voltage (kV)	Sintered side	Sheet resistance (Ω/sq)
Photon-sintered (printed samples are not pre-dried)	1	2 000	3.0	Coating	Uneven sintering
	2	2 000	2.0	Coating	Burnt
			3.0	Film	
	2	2 000	2.5	Coating	0.277
			2.5	Film	
	2	2 000	2.0	Coating	0.308
			2.5	Coating	
	2	2 000	2.5	Coating	0.290
			3.0	Coating	
	2	1 000	3.0	Coating	0.305
			2.0	Coating	
	2	2 000	2.5	Coating	0.275
			2.5	Film	
Photon-sintered on samples pre-dried at 80 °C for 15 s	2	2 000	2.0	Coating	0.392
		1 000	3.0	Film	
	2	2 000	2.5	Coating	0.260
			2.5	Film	
	2	2 000	2.0	Coating	0.349
			2.5	Coating	
	2	2 000	2.5	Coating	0.320
			3.0	Coating	
	2	2 000	2.5	Coating	0.222
			2.5	Film	

Initially, the sintering trials were done with rectangular bars and a sheet resistance of rectangular bar was measured to analyze the sintering performance. The distance and cover lid material have been kept constant as 10.5 inches and Pyrex, respectively. The power was changed to three different level: 3 kV, 2.5 kV, and 2 kV. These three power levels can be considered as High, Medium and Low power levels, respectively. We cannot go lower than 2 kV power using the Xenon S-2100a photonic sintering.

The printed side can be mentioned as coating side and non-printed side as film side. The two-sided sintering and two-pass sintering are done for two different voltage conditions. The sintering is performed for wet samples and samples pre-dried using oven sintering at 80 °C for 15 s. The sheet resistance obtained for different sintering conditions is shown in Table 7, Table 8, and Table 9, respectively.

The optimum conditions for the PET sample (3 kV, 10.5 inches) brought uneven sintering for BOPP sample. Then, two-sided sintering is performed with 2 kV (Low) for coating side and 3 kV (High) for film side which also resulted in the burnt sample. The voltage is then reduced to medium (2.5 kV) and two-sided sintering is performed and a low-resistance sintered sample is obtained. The sheet resistance obtained for non-pre-

dried and predried samples printed using 'SHR-2' ink for varying pulse width and voltage is shown in Table 7 and it can be seen that the minimum sheet resistance is obtained for sintering of coating and film side with 2.5 kV (Medium) and 2 000 µs pulse width, which is highlighted by the grey background.

The obtained sheet resistance values for both 'SHR-1' and 'SHR-4' inks are also lowest for the same conditions (two-sided sintering with the medium voltage at 2 000 µs pulse width) as seen in Table 8 and Table 9, also highlighted by the grey background.

The interpretation of microwave performance in terms of RCS amplitude and bandwidth of RFID tag sintered using photon sintering and oven sintering is shown in Table 10. The photon sintering of samples printed using 'SHR-2' ink reduced the bandwidth to 220 MHz with RCS amplitude of 12.42 dB, which is comparable to the response obtained from oven sintering. The sheet resistance has decreased by 0.1 Ω/sq compared to one-sided sintering performed in the previous section. In case of 'SHR-1' ink, the response of the printed tag is rather enhanced for the photon-sintered sample as oven sintering is limited to 80 °C for BOPP substrate. This can be related to the sheet resistance decrement by 0.5 Ω/sq for the photon-sintered sample. The samples printed using 'SHR-4' ink have higher thickness compared to

Table 8: Photon sintering of samples printed using 'SHR-1' ink on BOPP DCP substrate with two passes (distance = 1.5 inches from the lamp)

Sintering condition	Pulse width (µs)	Voltage (kV)	Sintered side	Sheet resistance (Ω/sq)
Photon-sintered only (printed samples are not pre-dried)	2 000	2.0	Coating	0.752
	1 000	3.0	Film	
	2 000	2.5	Coating	0.476
		2.5	Film	
	2 000	2.0	Coating	0.734
		2.5	Coating	
	2 000	2.5	Coating	0.605
		3.0	Coating	
	2 000	2.5	Coating	0.526
		2.5	Film	
Photon-sintered on samples pre-dried at 80 °C for 15 s	2 000	2.0	Coating	0.759
	1 000	3.0	Film	
	2 000	2.5	Coating	0.526
		2.5	Film	
	2 000	2.0	Coating	0.711
		2.5	Coating	
	2 000	2.5	Coating	0.608
		3.0	Coating	
	2 000	2.5	Coating	0.506
		2.5	Film	

Table 9: Photon sintering of samples printed using 'SHR-4' ink on BOPP DCP substrate with two passes (distance = 1.5 inches from the lamp)

Sintering condition	Pulse width (µs)	Voltage (kV)	Sintered side	Sheet resistance (Ω/sq)
Photon-sintered only (printed samples are not pre-dried)	2 000	2.0	Coating	Uneven sint.
	2 000	3.0	Film	
	2 000	2.5	Coating	0.277
		2.5	Film	
	2 000	2.0	Coating	0.349
		2.5	Coating	
	2 000	2.0	Coating	0.398
	1 000	3.0	Coating	
	2 000	2.5	Coating	0.313
		2.5	Film	
Photon-sintered on samples pre-dried at 80 °C for 15 s	2 000	2.0	Coating	0.392
	1 000	3.0	Film	
	2 000	2.5	Coating	0.265
		2.5	Film	
	2 000	2.0	Coating	0.389
		2.5	Coating	
	2 000	2.5	Coating	0.359
		3.0	Coating	
	2 000	2.5	Coating	0.252
		2.5	Film	

Table 10: Microwave performance of circular ELC resonator sintered using photon-sintering and oven-sintering procedures

Ink	Sintering method	Sheet resistance (Ω/sq)	Bandwidth (MHz)	RCS amplitude (dB)
SHR-2	Photon-sintered only (not pre-dried)	0.275	230	12.42
	Photon-sintered (pre-dried 80 °C for 15 s)	0.222	220	12.42
	Oven-sintered (80 °C for 10 min)	0.385	230	12.47
SHR-1	Photon-sintered only (not pre-dried)	0.526	290	8.16
	Photon-sintered (pre-dried 80 °C for 15 s)	0.506	270	9.38
	Oven-sintered (80 °C for 10 min)	1.076	350	7.17
SHR-4	Photon-sintered only (not pre-dried)	0.313	320	8.41
	Photon-sintered (pre-dried 80 °C for 15 s)	0.252	360	6.75
	Oven-sintered (80 °C for 10 min)	0.288	220	13.95

other inks as shown in Table 6, which can be the reason to have better performance for oven-sintered sample compared to photon-sintered sample. The higher thickness of 'SHR-4' ink might have been sintered more uniformly using oven sintering than photon sintering.

Hence, the photon sintering has shown improvement for RFID tag printed using 'SHR-1' ink. The microwave performance for sample printed using 'SHR-2' ink is similar for oven-sintered and photon-sintered sample. However, oven-sintered printed sample using 'SHR-4' ink is better compared to photon-sintered sample because of higher layer thickness. A high-speed photonic curing system is applicable for chipless RFID printed system and can be readily used to manufacture workable tag using fast roll-to-roll printing process.

5. Effect of the printed tracks dimensions on electrical parameters

The resistance of printed track depends on ink material composition, printing technology and geometrical dimensions (Bonea, et al., 2012). The wider line is less resistive and has higher conductivity based on the experimental investigation shown in Figure 12.
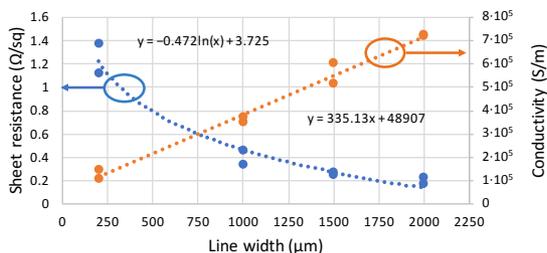
Figure 12: Sheet resistance and conductivity for varying line width of the track printed using 'SHR-2' ink

This is because the homogeneity of the conductive layer is better for the wider strip. It is seen that the conduc-

tivity gets decreased by $5 \cdot 10^5$ S/m when the line width is decreased from 2 000 μm to 200 μm. However, the conductivity in the range of 10^5 is still maintained for the narrowest strip of 200 μm line width. The resistance should be low enough even for narrower strips to obtain detectable microwave response. The fitted relationship between sheet resistance and conductivity, respectively, and the line width is shown in Equations [2] and [3], which can be used to predict the printed line conductivity for different line widths (in μm).

$$Sheet\ resistance = -0.472 \ln (linewidth) + 3.725 \quad [2]$$

$$Conductivity = 335.13 \times linewidth + 48907 \quad [3]$$

The experimental investigation performed in previous paragraph showed that the conductivity of printed strip is dependent on the ink width and the deposited ink thickness. The geometrical dimensions, i.e. the line length, width and ink thickness give the total amount of ink volume of a printed strip. This section investigates the effect of overall ink volume on the conductivity of the printed strip. The sheet resistance and conductivity of strip printed using 'SHR-2' ink of varying ink volume are depicted in Figure 13.
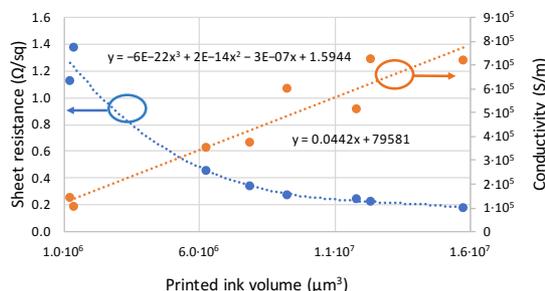
Figure 13: Sheet resistance and conductivity of strip printed using 'SHR-2' ink of varying ink volume

The conductivity is directly proportional to the printed ink volume, which indicates that the bigger tag design

with higher ink deposition has better conductivity compared to compact tag design. The chipless tag design is moving towards the development of smaller tags in order to have higher spatial efficiency. In case of the printed version of the chipless tag, the smaller tags can suffer because of low conductivity based on the relationship shown in Figure 13.

6. Printed samples accuracy

This section investigates the line width and gap width uniformity for printed samples on BOPP and PET substrate. The printed line width and the gap width of the chipless tag are measured using a Leica DM2500 microscope. The actual line width and gap width of the tag are 300 μm and 200 μm, respectively. The line width and the gap width of the resonator can vary after printing because of ink spreading or low ink flow. The width discrepancy for measured line width of 300 μm and gap discrepancy for measured gap width of 200 μm, are calculated using measured printed widths. The measurement is done for chipless tags printed on PET and BOPP substrate and the obtained discrepancy is shown in Figure 14.


(a)

(b)
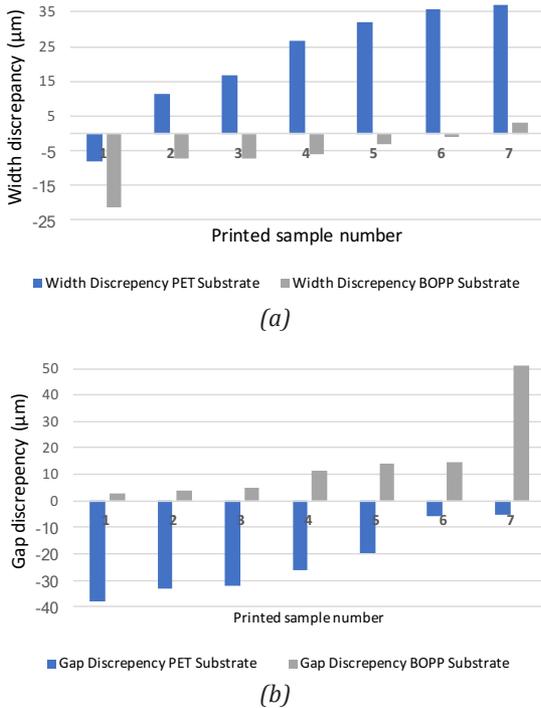
Figure 14: Line width (a) and gap width (b) discrepancy for RFID tags printed on PET and BOPP

In case of PET, the most part of the resonator has width widening causing a smaller gap (hence negative for gap discrepancy value) with the maximum of width increment of 37 μm. In the case of BOPP, the printed

lines have lower width than is the designed width of the sample, increasing the gap compared to the desired one. The deviation of the width increasingor gap narrowing in PET is lower compared to BOPP which can be because of the higher adhesion to PET. The reason behind the inconsistent discrepancy in line width and gap width can be because of variation in printing pressure, ink amount, and substrate flatness during manual screen printing. The automatic screen printing is able to minimize this discrepancy to a certain extent.

The resonant frequency of the tag is dependent on the equivalent inductance and the capacitance of the printed strip and the change in line width or the gap width of the printed strip can bring the change in resonant frequency. For instance, in BOPP printed sample number 1, the width is varied by 20 μm as seen in Figure 14(a). So, the simulation of the 1-bit RFID tag for the width of 280 μm and 300 μm is performed in Figure 15. The frequency shift is seen and hence printing accuracy is essential for detecting correct tag identification in printed RFID tag.
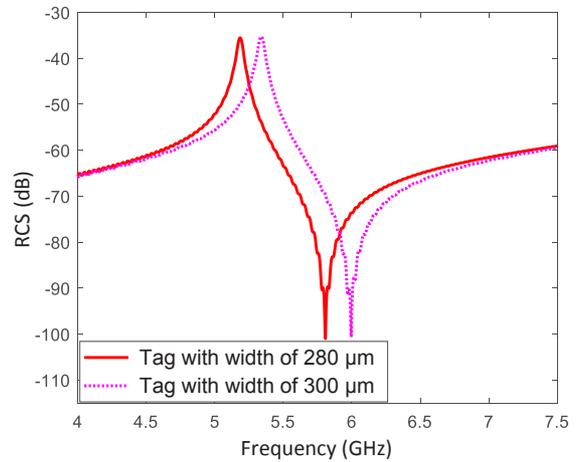
Figure 15: Response of the chipless RFID tag with different widths

We can assume the average line width broadening as *IncWidth* and decreased gap width as *DecGap* and consider these values in next print with smaller line width and reprint them to have the desired width. Hence, the adjusted line width and gap width can be obtained from Equations [4] and [5], respectively. For instance, for circular tag printed on PET, the average width broaden ing *IncWidth* is 21.65 μm and average gap decrease *DecGap* is 22.87 μm. These values can be considered in a new print to obtain required resonator dimensions.

New line width = Old line width – IncWidth　　[4]

New gap width = Old gap width + DecGap　　[5]

7. Relationship between printed tag response and printing parameters

This section will summarise the understanding obtained from the experimental analysis performed in the previous section and propose a general guidelines for printing of chipless tags. The microwave performance of printed chipless RFID tag is dependent on various printing parameters. A dependency chart showing the inter-relationship between the various printing parameters and the microwave performance of the printed tag is shown in Figure 16.

The microwave performance of printed tag is mainly dependent on four parameters: deposited ink thickness, ink conductivity, printing accuracy, and substrate parameters. The deposited ink thickness is dependent on the printing method and ink viscosity. The ink with higher viscosity can deposit higher ink thickness. However, the printing technique also determines the viscosity of the ink. The higher ink thickness is required for better RF response as explained in Section 2.
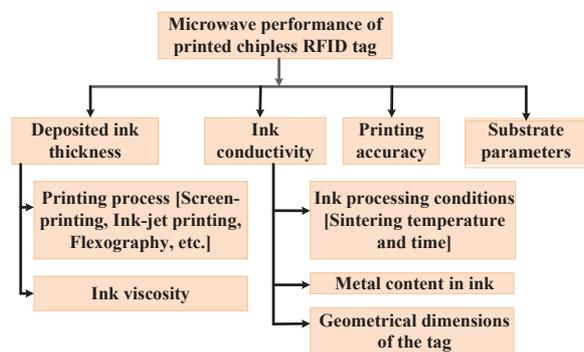

Figure 16: Relationship between the parameters involved in the printing of chipless RFID tag with its microwave performance

The screen-printing process can deposit a higher amount of ink compared to other printing processes. However, multiple passes can be printed in other print-ing processes to increase the deposited ink thickness. The printing process needs to be automatic to implement the multiple-pass print. Also, the excess amount of ink can create ink smudging and ink overflow creating unnecessary shorting. So, the ink viscosity needs to be optimal to print strip with higher thickness and better accuracy.

The low conductivity of ink broadens the microwave signal of the printed tag and also decreases the signal strength. Based on the experimental analysis higher sintering temperature can remove a greater amount of resistive component from the ink, forming highly conductive printed lines. However, the sintering temperature is limited by the physical properties of the substrate. The amount of metal content also has an influence on the ink conductivity.

Therefore, the bandwidth broadening for printed RFID tag can be minimized by using conductive ink which can give high conductivity at low sintering temperature for the oven sintering process. This will allow having printed RFID tag on a substrate with a low melting point. The photon sintering process can be adapted to have fast sintering for these substrates.

The geometrical dimensions (printed area) have a significant effect on the conductivity of the printed line according to the experimental investigation. The compact size tag is required to have higher bit capacity in the smaller area, which needs high resolution of printing. The digital printing technique such as ink-jet printing is able to print fine lines compared to the screen-printing technique. The multiple passes of print need to be employed to have higher ink thickness deposition which will reduce the resistance and minimize the signal loss as explained in Section 2. The printing accuracy is also important to obtain desired microwave response. The resonators are usually detuned using shorting at different locations. The printing inaccuracy due to ink overflow can create unwanted shorting in these locations and detune the resonator resulting in

Table 11: Issues, reasons, and solutions of the printed tags

Issue	Reason	Solution
Bandwidth broadening (low spectral efficiency)	Low ink conductivity	Ink sintered at a higher temperature for oven sintering or two-sided photon sintering
	Low metal content	Select ink with solid content >50 %
Low signal strength (RCS amplitude)	Low ink layer thickness	Screen print can deposit higher thickness or use multiple passes for other printing technologies
	Low ink viscosity	Increase the ink viscosity
The need of larger print dimensions	Low ink conductivity	Use ink with high conductivity
Printed dimensions inaccuracy	Printing technology	Use of digital printing technology; print the resonator with adjusted dimensions (considering the offset due to printing)

the false negative of the tag ID. The uniformity of line width in all sections of the printed resonator can also get affected because of printing inaccuracy which can result in false tag ID or absence of tag ID.

The screen-printing technique is prone to printing inaccuracy compared to other printing techniques. The printing accuracy can be enhanced by determining the change in printed dimensions and incorporating it in next print. The digital printing process such as ink-jet printing technique can be adapted to have better accuracy in printed dimensions. The summary of the analyzed issues of the printed RFID tag with their reason and the solution is shown in Table 11.

8. Conclusion

The printable chipless RFID tag combining the use of high-throughput printing processes and low-cost substrates such as a polymer is the most viable option to obtain extremely inexpensive RFID tags (0.1 cents/tag). The electromagnetic signature of the printed RFID tag suffers because of unavoidable limitation of printing technology. However, the performance of the printed chipless RFID tags can be improved by understanding the bottlenecks of the manufacturing procedure of printed tags. The microwave performance of the printed tags is dependent on parameters involved in their fabrication. The relationship between the printing parameters and the microwave response was analysed comprehensively in this paper, to understand the reasons behind the issues related to printed RFID tag. The dependency of parameters involved in the printing of chipless tag with its microwave response is deduced in the final section to elaborate the relationship and propose a viable solution to enhance the detection from the printed tag. An optimum printing setup, giving the workable tag response, can be deduced with the aid of this relationship which will eventually assist in obtaining a detectable and consistent response from the printed tag. The photon sintering of the chipless RFID tag is performed for the first time, to verify its suitability and obtain optimum conditions which can give the best microwave response. The photon sintering process can support sintering in a few seconds, making it suitable for the commercial roll-to-roll process of manufacturing printed items. This process can sinter the printed tracks at a temperature higher than the melting point of the substrate.

References

Balbin, I. and Karmakar, N.C., 2009. Phase-encoded chipless RFID transponder for large-scale low-cost applications. *Microwave and Wireless Components Letters, IEEE,* 19(8)**,** pp. 509–511.

Bonea, A., Brodeala, A., Vlădescu, M. and Svasta, P., 2012. Electrical conductivity of inkjet printed silver tracks. In: *2012 35th International Spring Seminar on Electronics Technology (ISSE 2012)*. Bad Aussee, Austria, 9–13 May 2012. IEEE, pp. 1–4.

Borgese, M., Dicandia, F.A., Costa, F., Genovesi, S. and Manara, G., 2017. An inkjet printed chipless RFID sensor for wireless humidity monitoring. *IEEE Sensors Journal,* 17(15), pp. 4699–4707.

Chamarti, A. and Varahramyan, K., 2006. Transmission delay line based ID generation circuit for RFID applications. *IEEE Microwave and Wireless Components Letters,* 16(11)**,** pp. 588–590.

Das, R. and Harrop, P., 2010. Printed and chipless RFID forecasts, technologies & players. [online] Available at: <https://www.idtechex.com/research/reports/printed_and_chipless_rfid_forecasts_technologies_and_players_2009_2019_000225.asp> [Accessed September 2018].

Forouzandeh, M. and Karmakar, N.C., 2015. Chipless RFID tags and sensors: a review on time-domain techniques. *Wireless Power Transfer,* 2(2), pp. 62–77.

Genovesi, S., Costa, F., Monorchio, A. and Manara, G., 2014. Phase-only encoding for novel chipless RFID tag. In: *2014 IEEE RFID Technology and Applications Conference (RFID-TA)*. Tampere, Finland, 8–9 September 2014. IEEE, pp. 68–71.

Genovesi, S., Costa, F., Monorchio, A. and Manara, G., 2016. Chipless RFID tag exploiting multifrequency delta-phase quantization encoding. *Antennas and Wireless Propagation Letters,* 15, pp. 738–741.

Halonen, E., Viiru, T., Ostman, K., Cabezas, A.L. and Mäntysalo, M., 2013. Oven sintering process optimization for inkjet-printed Ag nanoparticle ink. *IEEE Transactions on Components, Packaging and Manufacturing Technology,* 3(2), pp. 350–356.

Herrojo, C., Mata-Contreras, J., Paredes, F., Núñez, A., Ramon, E. and Martín, F., 2018. Near-field chipless-RFID tags with sequential bit reading implemented in plastic substrates. *Journal of Magnetism and Magnetic Materials,* 459, pp. 322–327.

Huang, H.-F. and Su, L., 2017. A Compact Dual-Polarized Chipless RFID Tag by Using Nested Concentric Square Loops. *IEEE Antennas and Wireless Propagation Letters,* 16, pp. 1036–1039.

Jeon, D., Kim, M.-S., Ryu, S.-J., Lee, D.-H. and Kim, J.-K., 2017. Fully printed chipless RFID tags using dipole array structures with enhanced reading ranges. *Journal of Electromagnetic Engineering And Science,* 17(3), pp. 159–164.

Khan, M.M., Tahir, F.A. and Cheema, H.M., 2016. Frequency band utilization enhancement for chipless RFID tag through place value encoding. In: *2016 IEEE International Symposium on Antennas and Propagation (APSURSI)*. Fajardo, Puerto Rico, 26 June–1 July 2016. IEEE, pp. 1477–1478.

Lukacs, P., Pietriková, A. and Cabuk, P., 2017. Dependence of electrical resistivity on sintering conditions of silver layers printed by inkjet printing technology. *Circuit World,* 43(2), pp. 80–87.

Mandel, C., Schüßler, M., Nickel, M., Kubina, B., Jakoby, R., Pöpperl, M. and Vossiek, M., 2015. Higher order pulse modulators for time domain chipless RFID tags with increased information density. In: *2015 45th European Microwave Conference (EuMC)*. Paris, 7–10 September 2015. EuMA, pp. 100–103.

Naqui, J., Coromina, J., Martín, F., Horestani, A. K. and Fumeaux, C., 2014. Comparative analysis of split ring resonators (SRR), electric-LC (ELC) resonators, and S-shaped split ring resonators (S-SRR): potential application to rotation sensors. In: M. Essaaidi, ed. *Proceedings of 2014 Mediterranean Microwave Symposium (MMS2014)*. Marrakech, Morroco, 12–14 December 2014. IEEE.

Noor, T., Habib, A., Amin, Y., Loo, J. and Tenhunen, H., 2016. High-density chipless RFID tag for temperature sensing. *Electronics Letters,* 52(8), pp. 620–622.

Preradovic, S. and Karmakar, N.C., 2009. Design of fully printable planar chipless RFID transponder with 35-bit data capacity. In: *European Microwave Week 2009, EuMW 2009: Science, Progress and Quality at Radiofrequencies, Conference Proceedings – 39th European Microwave Conference, EuMC 2009*. Rome, Italy, 28 September – 2 October 2009, pp. 13–16.

Sajitha, V.R., Nijas, C.M., Roshna, T.K., Vasudevan, K. and Mohanan, P., 2016. Compact cross loop resonator based chipless RFID tag with polarization insensitivity. *Microwave and Optical Technology Letters,* 58(4)**,** pp. 944–947.

Schroder, K.A., 2011. Mechanisms of photonic curing™: processing high temperature films on low temperature substrates. In: M. Laufon and B. Romanowicz, eds. *NSTI Nanotech 2011 proceedings: Vol. 2, Nanotechnology 2011: electronics, devices, fabrication, MEMS, fluidics and computational*. Boca Raton: CRC Press, pp. 220–223.

Vena, A., Babar, A.A., Sydänheimo, L., Tentzeris, M.M. and Ukkonen, L., 2013. A novel near-transparent ASK-reconfigurable inkjet-printed chipless RFID tag. *IEEE Antennas and Wireless Propagation Letters,* 12, pp. 753–756.

Vena, A., Sydanheimo, L., Ukkonen, L. and Tentzeris, M.M., 2014. A fully inkjet-printed chipless RFID gas and temperature sensor on paper. In: *2014 IEEE RFID Technology and Applications (RFID-TA) Conference*. Tampere, Finland, 8–9 September 2014. IEEE, pp. 115–120.

XENON Corporation, 2010. *Xenon S-2100: Rack-Mounted Sintering System*. [online] Available at: <https://www.polytec.com/fileadmin/d/Klebeprodukte/S-2100_SellSheet__1_.pdf> [Accessed September 2018].

Zomorrodi, M., 2015. *mm-wave EM-imaging chipless RFID system.* Ph.D. Thesis. Monash University.

TOPICALITIES

Edited by Markéta Držková

CONTENTS

News & more

An update on ISO standards for graphic technology

Here is the regular autumn summary of changes in ISO standards developed by ISO technical committee TC 130 Graphic technology during the last year since October 2017. Currently, there are almost forty standards in preparatory stages, for example, the standards within ISO 12643 series (Graphic technology – Safety requirements for graphic technology equipment and systems), from which two standards are in the stage of the final draft. These are ISO/FDIS 19302 Graphic technology – Colour conformity of printing workflows and ISO/FDIS 21632 Graphic technology – Determination of the energy consumption of digital printing devices including transitional and related modes. The new standard ISO 20294 Graphic technology – Quantification and communication for calculating the carbon footprint of e-media is under publication.

The standards which were reviewed and confirmed include ISO 2836:2004 Graphic technology – Prints and printing inks – Assessment of resistance of prints to various agents (confirmed this March and now again under review as a standard to be revised), ISO 5776:2016 Graphic technology – Symbols for text proof correction (with the next, third edition under preparation), ISO 11084-1:1993 Graphic technology – Register systems for photographic materials, foils and paper – Part 1: Three-pin systems (for the fourth time), ISO 12639:2004 Graphic technology – Prepress digital data exchange – Tag image file format for image technology (TIFF/IT), ISO 12640-2:2004 Graphic technology – Prepress digital data exchange – Part 2: XYZ/sRGB encoded standard colour image data (XYZ/SCID), ISO 15790:2004 Graphic technology and photography – Certified reference materials for reflection and transmission metrology – Documentation and procedures for use, including determination of combined standard uncertainty, ISO 15930-3:2002 Graphic technology – Prepress digital data exchange – Use of PDF – Part 3: Complete exchange suitable for colour-managed workflows (PDF/X-3), with the last four confirmed for the third time. Further, the corrected version of ISO 20654:2017 Graphic technology – Measurement and calculation of spot colour tone value is available since January 2018, with final Introduction paragraph removed and Formula (6) revised.

ISO 12636:2018
Graphic technology – Blankets for offset printing

The original version from 1998 was technically revised and published this January as a second edition. The standard specifies requirements on blankets for offset printing, except the un-tensioned or unclamped ones and offset printing sleeves used on gapless presses. The test methods for determination of corresponding characteristics are provided, including blanket thickness, elongation, tensile strength, load at specific deflection, compressibility in terms of average thickness reduction (deflection) as well as average depth of impression (indentation), surface texture, and thickness change (swelling or shrinkage) after exposure to a test liquid and after recovery from this exposure. Here the standard also defines exposure conditions for printing ink ingredients and washes. Further, the ordering and labelling information is specified.

CORNET
Collective Research Networking

While originally launched as an ERA-NET in 2005 and supported by the European Commission's 6th and 7th Framework Programme for Research and Development, CORNET is a self-sustained network since January 2011, based on national or regional funding schemes and available budgets. Its aim is to increase the competitiveness of small and medium-sized enterprises by funding international pre-competitive Collective Research projects. The research results are widely published which enables a large number of enterprises benefitting from one project. For example, the project POLEOT – Printing of Light Emitters on Textile funded from 2013 to 2015 is listed among the success stories. The present European CORNET partners come from Austria, Belgium, Czech Republic, Germany, Netherlands, Poland and Switzerland, with partners from Canada, Japan and Peru outside Europe. Calls for proposals for international Collective Research projects are issued by CORNET twice a year.

New Master of Engineering degree in Printed Intelligence

The Oulu University of Applied Sciences now offers the new Degree Programme in Printed Intelligence, with the studies beginning in spring 2019. The curriculum includes Project management, Quality management, Virtual business simulation and management, Printed electronics, Printed electronics methods and applications, Printed intelligence product development, and Master's thesis project. Besides the online studies, intensive contact teaching periods are planned.

A decade of PrintoCent

The PrintoCent innovation centre was founded in 2009. In 2012, the pilot factory for printed intelligence industrialisation was opened at the VTT Technical Research Centre of Finland premises. It is complemented by PrinLab – Development laboratory for Printed Intelligence at the Oulu University of Applied Sciences, utilising different printing techniques in sheet and roll-to-roll processes, and laboratory-scale machines and testing devices at the Oulu University. The open-access environment of the PrintoCent Pilot Factory with roll-to-roll and hybrid manufacturing capabilities enables companies to up-scale the new technology based on the pilot-scale manufacturing trials and support in factory planning and construction, machinery selection, product technical design and device integration, production ramp-up support, quality and performance audits, and more. Application focus areas include e.g. rapid disposable diagnostics, smart flexible lighting, wearables and energy harvesting.

The PrintoCent Industrial Cluster has about 40 member companies from start-up and micro companies over small and medium-sized enterprises up to large global companies, representing different parts of the value chain. The PrintoCent Innovation Accelerator covers the activities connected to the availability of relevant education and resources, excellence and strong co-operation in research, open Innovation events and the PRINSE seminar organised every second year. The 5th PrintoCent InnoFest event for teams competing on their ideas with the help of researchers and company experts took place in Oulu at the beginning of June 2018. This year over half of the InnoFest participants came from companies. The first prize was awarded to the team that came up with the business case based on a digital device for saliva analysis as a portable diagnostic tool for measurement of vitamin intake or blood level.

ISO 17972-4:2018
Graphic technology – Colour data exchange format (CxF/X)
Part 4: Spot colour characterisation data (CxF/X-4)

Compared to the first version of the document from 2015, the main changes in the second edition from this January comprise the corrected electronic files for Annexes A and B (XML schema for CxF/X-4 CustomResource and Examples of CxF/X-4 documents, respectively), clarification in the section defining printed patches regarding the requirement that the set of patches printed on the region printed with black ink shall have the same tint levels as the set of patches printed on the unmarked substrate, and adding a possibility to prepare the black region using a combination of inks. Otherwise, the exchange format for spectral measurement data of spot colour inks, i.e. the definitions of general requirements, conformance levels, characterisation chart preparation and measurement communication, remains unchanged.

ISO 19593-1:2018
Graphic technology – Use of PDF to associate
processing steps and content data
Part 1: Processing steps for packaging and labels

The new standard published this July defines standardised mechanisms to store graphics objects and metadata corresponding to the processing steps of printed products in a PDF file with the aim of improving interoperability between companies and systems – see also Ghent Workgroup specification 'Storing Processing Step Data in PDF' in JPMTR 5(2016)4. The standard covers both the generic requirements and those specific for packaging and labels. The method is based on collecting all objects belonging to the same processing step in a corresponding Optional Content Group (OCG) and including the metadata that identify given processing step. The requirements on colouring and positioning of processing-step objects both in off-bleed areas and when they are allowed to overlap with print content are specified, together with limitations on processing-step PDF objects describing paths and surfaces. For packaging and labels, the groups for processing-step OCGs include structural data (CAD) corresponding to finishing steps, such as cutting, folding or glueing, braille for braille text, legend for administrative and technical information panels, dimensions for dimension lines and indications of physical size, positions for positioning information of various elements, white for description of a printed white backing, and varnish for objects describing printed varnish.

ISO 20690:2018
Graphic technology – Determination of the operating power
consumption of digital printing devices

Available since February 2018, this new standard enables energy efficiency assessment for both small-format and wide-format digital production printing presses (also called professional digital printing presses) including peripheral devices. A method for the estimation of energy efficiency, expressed in numbers of A4 pages per kWh or in m^2/kWh for a large-format system, is based on requirements and recommendations for measuring the electricity consumption in different modes of operation. Power measurement is specified for print production mode as well as for print waiting modes (Off, Print Ready, Sleep). The devices being compared based on the results acquired according to this standard should be set up to produce the same print quality using comparable types of printing technology, process and device configurations.

Bookshelf

Camera Image Quality Benchmarking

The current advances in imaging technology, from digital single-lens reflex (DSLR) cameras over cutting-edge mobile imaging to sophisticated image processing, require the corresponding development in image quality assessment so that the imaging industry can compare and rate various imaging systems. This book was written to describe a methodology for a complete characterisation and benchmarking of present cameras, considering combined aspects of image quality for both still and video imaging applications. Besides the objective metrics based on measurements independent of human perception, also the metrics reflecting the subjective experience of image quality have been developed by the interested initiatives and standards bodies to meet the need for standard benchmarking metrics that provide consistent, reproducible, and perceptually correlated results. The authors review the essential elements of image quality and the methods for their evaluation, together with the techniques correlating perception-independent measurement results with the subjective ones. They also discuss practical aspects of setting up a laboratory for image quality characterisation, as well as benchmarking approaches and considerations, supported by example data. The companion website includes animated GIFs and videos illustrating issues with automatic exposure, focus and white balance, aliasing, ghosting, rolling shutter, stabilisation, etc.

The introduction explains the relationship between the content of an image and its quality, presenting the characteristics important for realistic imaging – colour, shape, texture, depth, luminance range, and motion. It also explores the task of image quality benchmarking and outlines the remaining book content. Chapter two defines image quality itself, its attributes and their categorisation, explaining also the difference between global and local attributes and pointing to the specifics of subjective and objective image quality assessment. The image quality attributes of both still images and video are then explored in the next chapter in more detail. Chapter four describes the components and architecture of a digital camera, establishing the connection between each component with its key parameters and the image quality attributes. The following two chapters deal with the theory and practice of subjective and objective image quality assessment, respectively. Key psychometric techniques for quantifying subjective image quality are reviewed, such as category scaling, forced-choice comparisons, acceptability ratings and mean opinion score, with a particular focus on the anchor scale method and its use in quantifying overall image quality based on just noticeable differences of various attributes. In the case of objective metrics, also the practical measurement issues are discussed. Chapter seven discusses two fundamental approaches and a large number of methods for correlation of objective image quality metrics with perception. Then, the measurement protocols for both objective and subjective measurements are presented in chapter eight and the comprehensive camera benchmarking process in chapter nine, followed by the concluding chapter.
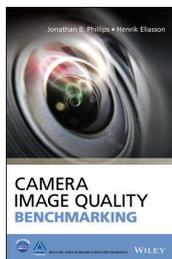
Authors: Jonathan B. Phillips, Henrik Eliasson

Publisher: Wiley
1st ed., January 2018
ISBN: 978-1-119-05449-8
396 pages
Hardcover
Available also as an eBook

Computing Colour Image Processing: Digital Colour Primer

Author: Alan Parkin

Publisher: Springer
1st ed., March 2018
ISBN: 978-3319740751
143 pages, 101 images
Softcover
Also as an eBook
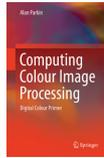
The approach to processing the colour information in digital images presented by the author of this book is based on his experience and attitudes. After the first two chapters introducing the basics of colour and digital imaging, the next two describe the ways of creating and storing a digital image. The main part of the book deals with location and colour transformations, displaying and printing an image, and finally with analysing and balancing image colour. The sRGB colour space and Python scripting are utilised in elementary tools provided for image processing following the described approach, e.g. to achieve neutral colour balance.

The Hologram: Principles and Techniques

Authors: Martin J. Richardson, John D. Wiltshire

Publisher: Wiley-IEEE Press
1st ed., November 2017
ISBN: 978-1119088905
330 pages, Hardcover
Also as an eBook
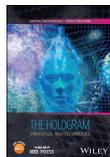
This thorough resource first explains what is – and also what is not – a hologram and overviews relevant optical principles. Next, the conventional holography and the digital image holograms are introduced, followed by a review of recording materials for holography and processing techniques. Further, a holography studio and its configurations for making different types of holograms are described. The ninth chapter deals with sources of holographic imagery, considering also the relationship between process

Introduction to Graphic Communication

This volume is an update to Harvey R. Levenson's book published in 2007, adding new insights and tracking the graphic communication developments of the past ten years. Besides the changes in the printed content, the book utilises integrated multimedia and supports peer-to-peer interaction.

After the first chapter defining what is graphic communication and what is covered in the book, the second one reviews the milestones in the history of printing or, more generally, of graphic communication. The third chapter examines the challenges connected with technological transitions, discussing which difficulties can companies encounter during the implementation of new technologies. This becomes more important as the development of new technologies accelerates. The fourth chapter goes through individual print industry segments and chapters five to nine then deal with the main production steps – design and prepress workflow, colour management and proofing, materials, i.e. paper, ink, and toner, printing processes, and postpress and finishing. The tenth chapter separately discusses the specifics of printed packaging. Chapter eleven is dedicated to best practices and industry standards. It shows the importance of proper job specification and describes the individual elements of print transaction that must be considered. The second part provides the list of organisations developing standards and specifications for the field of graphic communication. Finally, chapter twelve looks at the relationship between printing and the digital world, including digital assets management and multichannel publishing.

The book makes use of Ricoh's Clickable Paper and Viddler Training Suite to access related digital content. The library contains the introduction and summary comments for chapters, explanatory videos illustrating selected terms and principles, and also commercial presentations. In the last case, a greater diversity would be beneficial for the users to get a more complete picture. Some videos present research results, such as the one from Sappi with David Eagleman explaining 'How the medium shapes the message'. The book as a product is not perfect, with content partly hidden in the spine, missing references to sources, lower quality of some images and other flaws, such as ".com" missing in the links provided at the chapter beginnings and the chapter four summary containing the video that reviews the third one. Overall, the book delivers what the title promises – a solid overview of the graphic communication industry. The content will not satisfy those who search for a deeper theoretical background but it provides a comprehensive introduction for readers who are new to the field, clearly explaining the relevant terms related to printing materials, techniques, exchange of content data, and more. For the others it can serve as a reference adding some interesting details; for example, European readers can become more familiar with American classifications, such as in the case of bindings.

Review by Jan Vališ and Markéta Držková, University of Pardubice

Authors: Harvey Levenson, John Parsons

Publisher: IntuIdeas
2nd ed., April 2018
ISBN: 978-0-692-08117-4
248 pages
Softcover

Bookshelf – J. Print Media Technol. Res. 7(2018)3, 147–152

149
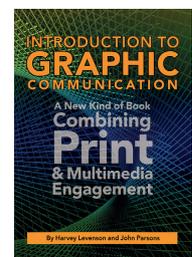
The Visual History of Type

Simply said, this large book written and designed by Paul McNeil was made for all who love type. The history of type from the half of 15th century until now is presented through carefully selected and well-reproduced specimens of more than three hundred typefaces, arranged chronologically. The illustrations in sufficient size and good quality show typefaces as early used in print or their original specimens, exemplifying various uses. Besides the major typefaces generally considered as classics, the selection contains also some typefaces which were used just for a short while, in order to truly reflect every era. Also for the present day, the typefaces that represent the important and interesting innovations are included.

This by itself would be enough – but this comprehensive resource brings more than that. A spread for each displayed typeface provides its concise history and lists available typeface details, key characteristics, connections to other typefaces, and also the current availability of the typeface. The book helps to explore the relationships and influences, putting the evolution of typefaces in context and showing the social impact of type. Altogether, this volume allows to gain insight and deepen understanding of typography.

Author: Paul McNeil

Publisher: Laurence King Publishing
1st ed., September 2017
ISBN: 978-1-78067-976-1
672 pages, 350 images
Hardcover

How to Create Typefaces:
From Sketch to Screen

This compact but rigorous book was originally published in Spanish in 2012 and since then it has been published in different languages and become a popular choice for those who want to learn about type design. The guide describes the principles and demonstrates the process and techniques used for creation of typefaces, highlights essential characters and explains the related terms. Attention is paid for example to the importance of consistency, optical corrections, spacing adjustments and considerations to be taken into account when designing typeface family. The book covers digitisation and work with digital outlines, as well as the overall role of digital technology, including the possibilities given by OpenType and Unicode. The legal issues and other distribution aspects are also considered. The authors show not only how to create a new typeface but also discuss the reasons why.

Authors: Cristóbal Henestrosa,
Laura Meseguer, José Scaglione

Publisher: Tipo e
1st ed., May 2017
ISBN: 978-84-938654-3-6
152 pages, 123 images
Softcover

colours and holography. Here, the methods for assimilating CMYK artwork with holography and for interpretation of CMYK separations in the RGB format are mentioned. The book ends with the authors' personal view of the history of holography and an overview of the impact of holography in the world of imaging.

The Rise and Fall
of the British Press

Author: Mick Temple

Publisher: Routledge
1st ed., September 2017
ISBN: 978-1138895102
114 pages
Hardcover
Also as an eBook

The author of this book follows the evolution of the British press through its whole history from the beginning to today, discussing the impact of new technology as well as the influences between the press, politics and society. The text covers the birth of the first mass medium, the role of press barons, the challenge of broadcasting, the long decline, the Wapping dispute – up to the current issues, including the local newspaper situation. The last two chapters deal with a fifth estate and the future scenarios of print journalism.

The Typographic Imaginary in
Early Modern English Literature

Author: Rachel Stenner
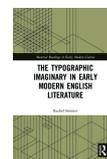
Publisher: Routledge
1st ed., June 2018
ISBN: 978-1472480422
216 pages, 5 images
Hardcover
Also as an eBook

This study describes the aesthetic links of authors from the mid-fifteenth to the mid-eighteenth centuries and proposes a new framework for an analysis of print culture, based on the work of writers who were more or less engaged in the print trade, with print seen not only as a tool but as a subject to address.

Handbook of Adhesion Promoters

Author: George Wypych

Publisher: ChemTec
Publishing
1st ed., March 2018
ISBN: 978-1927885291
242 pages, Hardcover
Also as an eBook

This book is a comprehensive review of an important group of additives used in many industrial products. It explains mechanisms of adhesion and adhesion loss. Then it deals with surface condition and treatment of substrates and presents typical primer formulations and applications to different substrates. Here also the formulations of primer coating for paper and printing are covered. In the latter case, the examples comprise two primers for increased adhesion of liquid toner and a primer for the magnetically oriented ink used in security documents. Next, polymer modifications improving adhesion are discussed. The following chapters list properties of various adhesion promoters available on the market and assist in their selection for different substrates and products. Finally, the relationship of adhesion and corrosion protection is discussed.

Packaging for Nonthermal Processing of Food

Editors: Melvin A. Pascall, Jung H. Han

Publisher:
Wiley-Blackwell
2nd ed., June 2018
ISBN: 978-1119126850
320 pages, Hardcover
Also as an eBook

The second edition was revised and updated to reflect the changes that took place since the first publication in 2007, including the coverage of intelligent packaging, utilising e.g. various sensors, chromic materials or radio frequency identification, as well as an overview of current packaging laws and regulations. The influence of package design on consumer purchase intent is also discussed.

Photovoltaics:
Fundamentals, Technology and Practice

The second international edition of this textbook on photovoltaic technology brings updated information to reflect the current state of the art and the achieved efficiencies. There is also a new chapter dealing with the storage of solar energy, shortly introducing the basic principle, describing relevant types of batteries with their operating characteristics and discussing the role of storage in self-consumption applications, as well as the stand-alone systems. Further, the analysis of potential-induced degradation was included in the chapter on photovoltaic metrology and the chapter on future development in photovoltaics was expanded, reviewing e.g. the position of renewable energies in today's power supply system.

The supplemental materials are again available online at the accompanying website, including supporting software, downloadable figures and solutions of the exercises for individual chapters. The book is also published in German by Carl Hanser Verlag, currently in the fourth edition.

Author: Konrad Mertens

Publisher: Wiley
2nd ed., July 2018
ISBN: 978-1-119-40104-9
368 pages
Hardcover
Available also as an eBook
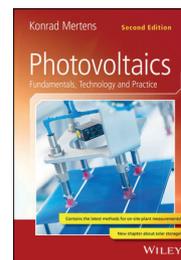
Advanced Mechanics of Composite Materials and Structural Elements

The authors of this book primarily aimed to cover mechanics, technology, and analysis of composite materials and structural elements at an advanced level, considering both the essential mechanical properties of the material itself and the special features of its practical implementation. The fourth edition with slightly modified title reflects new manufacturing processes, including 3D printing of two matrix composite structural elements, and presents new theories developed by the authors. The first three chapters describe mechanics of a unidirectional ply, a composite layer and laminates. Then, failure criteria and strength of laminates are discussed, as well as the environmental, special loading and manufacturing effects. The remaining part deals with typical composite structural elements, namely the laminated composite beams and columns, composite plates, thin-walled composite beams, circular cylindrical shells, including optimal lattice composite structures, composite shells of revolution, and composite pressure vessels.

Authors: Valery Vasiliev, Evgeny Morozov

Publisher: Elsevier
4th ed., June 2018
ISBN: 978-0-08-102209-2
882 pages
Softcover
Available also as an eBook

Bookshelf – J. Print Media Technol. Res. 7(2018)3, 147–152

151
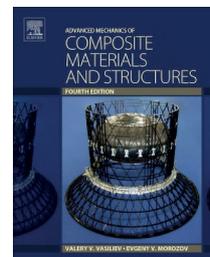
Bookshelf

Academic dissertations

Methods for Qualification of CCD Line Scan Cameras as a Measuring Device for Color and 3D Measurement

This thesis examined the performance of camera-based measuring instruments with respect to their suitability for process control in industrial environments based on the measurement accuracy that can be achieved with these systems. The methods developed and used within the scope of this thesis tested the abilities and limitations of two models of line-scan cameras for colour and 3D measurement, respectively. The dissertation reviews the relevant fundamental aspects of the CCD line sensors, camera-based colorimetry and stereoscopic 3D measurement. The first one of the three experimental chapters presents the setup for characterisation of the camera sensor with respect to its linearity and noise, introduces the measurement-based sensor model and discusses the influence of digitised signal discretisation. The chapter dedicated to a characterisation of the colour measurement system based on the multispectral line-scan camera details the measurement of the spectral system sensitivities and then discusses the consistency test of measured sensitivities and calibration, the extent of the empirical calibration validity, the influence of system noise and inhomogeneity of the measuring fields, as well as the simulation-based system analysis. Finally, the chapter dealing with a characterisation of the 3D surface topography measuring system utilising the stereo line-scan camera considers the frequency-dependent depth of field, describes the experimental setup and presents the determination of the modulation transfer function change by Fourier transformation. Then it analyses the important parameters and aspects, namely the axial chromatic aberration, field curvature, astigmatism, measurement noise, correlation window and the dominant object modulation frequency. The influence of the depth of field as an optical low-pass filter on the 3D surface measurement, and especially the influence of system noise, correlation window size and optical defocus on the 3D surface reconstruction are further discussed, followed by the overall summary.

Doctoral thesis – Summary

Author:
Maximilian Klammer

Speciality field:
Color Measurement

Supervisors:
Edgar Dörsam
Tran Quoc Khanh

Defended:
1 November 2017, Technical University of Darmstadt, Department of Mechanical Engineering, Institute of Printing Science and Technology Darmstadt, Germany

Language:
German

Contact:
doersam@idd.tu-darmstadt.de

Passive Thin Film Circuits of Nanomaterials, Inkjet Printed on Flexible Temperature Sensitive Substrates

The principal objective of the research in the area of printed electronics within this thesis was to produce passive electronic functionalities on flexible substrates without the need of thermal annealing at high temperature. Inkjet printing of inks based on nanoparticle dispersion was chosen to pattern low-resistance, semiconducting and dielectric traces. The dissertation covers the processing steps from preparation of functional inks through their multi-pass deposition using inkjet printing up to fabrication of planar circuit elements and vertically integrated multilayer components. It deals with the properties of 1D and 2D materials, the fluid attributes of the inks, the printing parameters influencing the deposition quality, the morphology of printed features, their electrical conductivity and its improvement by post-processing. The attention is paid to appropriate characterisation and discussion of the achieved results, with the engineering aspects and potential applicability for large-scale production naturally considered thanks to the author's background in the industry.

Doctoral thesis – Summary

Author:
David Joseph Finn

Speciality field:
Physics

Supervisors:
Jonathan N. Coleman
Plamen Stamenov

Defended:
7 November 2017, Trinity College Dublin, School of Physics Dublin, Ireland

Contact:
david.finn@amatechcorp.com

First, the electrical traces deposited using the piezoelectric inkjet printer with dispersed pristine graphene as the conductive ink showed resistivity that was too high to produce electrically functional graphene networks for application in passive high-frequency antenna circuits; nevertheless, an all-inkjet-printed photodetector with interdigitated graphene electrodes and a MoS_2 channel was successfully demonstrated. Next, good electrical properties were achieved in the case of silver nanowire networks prepared using piezoelectric inkjet printing as the deposition method, combined with thermal treatment. However, ageing was observed, most likely due to the damage of the surface passivation layer during the sonication process used to shorten the nanowires in order to prevent nozzle clogging. Further, electrostatic capacitors with a hybrid multilayer structure combining conducting graphene and dielectric hexagonal boron nitride were fabricated by inkjet printing and spray-casting. Finally, the thermal inkjet printing was used to pattern aqueous dispersions of silver platelets as the conductive ink. After a thermal treatment at 50 °C for 24 hours, the printed lines exhibited low sheet resistance. This enabled the fabrication of an innovative single-loop coupling frame printed by inkjet on a low-temperature substrate for application in radio-frequency identification dual-interface transaction cards.

Doctoral thesis – Summary

Author:
Nouran Yehia Adly

Speciality field:
Biosensors

Supervisors:
Bernhard Wolfrum
Marc Spehr

Defended:
23 March 2018, RWTH Aachen University, Faculty of Mathematics, Computer Science and Natural Sciences Aachen, Germany

Contact:
nouran.adly@tum.de

Inkjet-Printed Electrochemical Devices for Bioelectronics

The purpose of the research within this thesis was to create a new alternative platform for developing diagnostic tools with high sensitivity and low cost. The proposed approach for a detection of disease biomarkers and cardiac action potential using printed devices is clearly presented and based on three main elements. First, the controlled bioreceptor immobilization was achieved by the photonic immobilization on printed chips. Presented technique for site-specific immobilization of antibodies showed a higher sensitivity and better limit of detection compared to the conventional approaches. The first application comprised the determination of C-reactive protein in the presence of human serum. Second, signal amplification using electrochemical redox cycling was accomplished by the repetitive cycling of redox probes between two adjacent electrodes. To ensure a short distance between the electrodes required for an effective redox cycling amplification and thus the sufficient sensitivity, a new scheme for fabricating micro-gap electrodes with in-plane displacement was developed, as well as porous nano-gap electrodes with out-of-plane displacement. The technique employs inkjet printing without prior surface patterning. The use of micro-gap redox cycling sensors for the detection of single-stranded DNA using peptide nucleic acids immobilized on the carbon microelectrodes is demonstrated, as well as their application to the detection of human immunodeficiency virus HIV-1 marker sequence. The third element consists in the development of novel methodology for high-resolution printing, resulting from the study of different physical, chemical and hydrodynamical properties of an ink droplet interacting with a substrate surface. A rapid prototyping approach based on inkjet printing of gold and carbon inks was utilised for fabricating high-resolution microelectrode arrays on flexible substrates, showing good electrical and outstanding electrochemical characteristics suitable for cellular recording and stimulation, which was successfully proved by a series of in-vitro extracellular recordings of action potentials from different biological systems. Because a transparent and flexible microelectrode array is beneficial as a functional cell–device interface in the case of in-vivo applications, such as neuronal implants, high-resolution microelectrode arrays were also printed on different soft materials, including gummy bears representing gelatin-based substrates.

Events

45th International iarigai Conference
Advances in Printing and Media Technology:
From Printing to Manufacturing

Warsaw, Poland
3–7 October 2018

The iarigai conference is this year held together with the annual IC conference (see below). Both conferences are hosted by the Department of Printing Technology of the Warsaw University of Technology, celebrating in 2018 the 50th anniversary. The joint programme of iarigai and IC includes a plenary session on Friday 5 October. The announced speakers are Volker Jansen with the talk on 'The Impact of Digital Media Use on Education Purpose', Edgar Dörsam revealing the challenge of 'The world of printing – unlimited possibilities' and Martin Habekost presenting 'Metallic inks and the M3 measurement mode – just made for each other'. The Official Jubilee Session opens the joint programme on Saturday, followed by the second plenary session with keynotes on 'Smart factory – future of the graphic arts industry' by Ulrich Hermann, 'The results of the research of KPMG and PBKG – Modern printing market in Poland' by Jacek Kuśmierczyk, and 'Multidot – innovative offset screen' by Andrzej Kunstetter. Then a joint panel discussion is scheduled. In addition, the common social programme is organised to support networking of both organisations.

The programme of the iarigai conference offers a number of plenary and parallel sessions covering a broad range of topics – from design for print and online, over advances in materials, processes and products, up to the progress in print quality assessment and automation.

50th International Circle Conference

Warsaw, Poland
4–7 October 2018

The annual conference of the International Circle of Educational Institutes for Graphic Arts Technology and Management (IC) celebrates this year the same anniversary as the Department of Printing Technology of the Warsaw University of Technology. The joint plenary sessions organised together with the co-located iarigai conference and introduced above are complemented by the parallel sessions on Friday (5 October). Besides the lectures dealing with technology innovations, such as the use of NFC technology and augmented reality in smart packaging or adding value to print using enhanced digital printing, many contributions are focused on education and didactic issues. These include the critical analysis of the digital academic in a digital class, the discussion of interdisciplinarity in the teaching of graphic technology, namely for screen printing, digital printing and postpress, and the presentation of names and context in the case of classifications for graphic communication and media technology fields in education, industry and science.

WAN-IFRA events

The main events organised by WAN-IFRA in the last months of this year begin with the 2018 editions of IFRA World Publishing Expo and DCX Digital Content Expo, both taking place in Berlin, Germany on 9–11 October. The series of 2018 Digital Media conferences then continues in November, namely Digital Media Asia taking place in Tsim Sha Tsui, Hong Kong (7–9 November), Digital Media LATAM in Bogotá, Colombia (14–16 November), and Digital Media Africa in Johannesburg, South Africa (23 November). The latter two are accompanied by the corresponding Digital Media Awards 2018. Further, WAN-IFRA offers The Newsroom Summit 2018 in Oslo, Norway on 29–30 October, the Local Digital Subscription Summit in Frankfurt, Germany on 14 November, two study tours and several workshops.

Smithers Pira Events

The programme of Smithers Pira events for the fourth quarter of 2018 opens the US edition of Specialty Papers conference organised jointly with TAPPI in Appleton, Wisconsin, USA on 2–3 October. Four weeks later, Sustainability in Packaging Europe is held in Barcelona, Spain (on 30–31 October, with two pre-conference half-day sessions the day before). Next month, Food Contact Training in offered in Cleveland, Ohio, USA (13–14 November). Finally, two conferences are organised at the beginning of December. The first one is P&P – Plastics & Paper in Contact with Foodstuffs in Vienna, Austria on 3–6 December and the second one is the European edition of Digital Print for Packaging which takes place in Berlin, Germany on 4–6 December.

Paper & Beyond

Brussels, Belgium
16–17 October 2018

This event, being the new version of the European Paper Week, is organised by the Confederation of European Paper Industries (CEPI) as the meeting place for paper industry and EU policymakers. It starts in the afternoon of the first day with presentations of young researchers, finalists of the Blue Sky Young Researchers & Innovation Award Europe, and an announcement of the winners. This programme is complemented by two panel discussions. The sessions on the second day first deal with the circular bioeconomy and its markets and then with deep eutectic solvents for sustainable paper production.

Paper & Plastics Recycling Conference

Chicago, Illinois, USA
17–19 October 2018

This recycling industry conference and trade show is organised by the Recycling Today Media Group. The 2018 sessions of the North American edition cover e.g. the material trends in packaging and the impact of employing artificial intelligence in materials recovery facilities. The European edition is held in Prague, Czech Republic on 6–7 November.

2018 SGIA Expo

Las Vegas, Nevada, USA
18–20 October 2018

The printing trade exhibition of the Specialty Graphic Imaging Association offers in 2018 more than 70 educational sessions on technology, business management and production issues.

2018 NPIRI Fall Tech Conference

St. Charles, Illinois, USA
9–11 October 2018

This conference is one of the events organised by the National Printing Ink Research Institute (NPIRI) under the auspices of the National Association of Printing Ink Manufacturers (NAPIM) to provide the ink industry with the up-to-date technical information. After the pre-conference short course introducing to ink formulation and manufacturing, including material selection, testing and quality control, the main programme of 2018 conference starts in the afternoon of the first day by a keynote address of Ron Osborn discussing the issues related to compliance and safety of packaging materials. The following presentations then cover topics from supply chain and global import/export considerations, over report on the state of the industry and technical talks, presenting trends in the graphic communications, pure azo pigments, chemical characterization of modern food contact materials, LED UV curing, and printed substrates compostability, up to the regulatory legislation and related standards. This year, NAPIM/NPIRI partners with Ink World and Printed Electronics Now magazines. The new technology session on the third-day morning is shared with the Electronic and Conductive Ink Conference introduced below.

Electronic and Conductive Ink Conference

St. Charles, Illinois, USA
10–11 October 2018

The morning session of this new conference is organised jointly with the NPIRI Fall Technical Conference and features the keynotes on 'Conductive and electronic inks – driving the flexible electronics revolution' by David Savastano and 'Activegrid™: a flexible transparent conductor with outstanding optoelectronic properties' by Ajay Virkar. The following agenda consists of presentations on various conductive inks and printed electronics topics and also a panel discussion on electronic packaging for consumer brands.

TheIJC 2018
5th Annual InkJet Conference

Düsseldorf, Germany
16–17 October 2018

This annual event organized by ESMA, the European association for printing manufacturers in screen, digital and flexo technology, in 2018 again offers free afternoon inkjet workshops the day before and plenary sessions continued by three programme tracks on each conference day. The plenary talks scheduled on 16 October are 'Recirculating printheads for industrial applications' by Changlong Sun, 'Latest advances in Silicon MEMS printhead technologies' by Jason Remnant, 'Development of logic-based methodologies for quantitative and qualitative analysis of nozzle jetting and printhead performance' by Shane O'Neill, and 'Considerations for inkjet printhead selection' by Shin Ishikura. The plenary speakers for the second day are Dan Denofsky reviewing 'Continuous Inkjet printing for packaging and industrial applications', Ben Brebner presenting 'Powerdrop: making ink stick' and John Corrall introducing 'New printheads from Konica Minolta'.

American Printing History Association Annual Conference
Matrices: The Social Life of Paper, Print, and Art

Iowa City, Iowa, USA
25–27 October 2018

The 43rd APHA annual conference is held jointly with the Friends of Dard Hunter (FDH) at the University of Iowa Center for the Book (UICB). On the first conference day, the trade fair is set up and open to the public. The sessions scheduled on the next two days allow participants to choose from lectures, discussions and demonstrations on a range of topics, offering up to five concurrent options. The announced keynotes are 'Papermaking & printmaking collaborations' by Ruth Lingen and 'Printing the renaissance pop-up book' by Suzanne Karr Schmidt.

On 24 October, a one-day pre-conference tour 'Iowa Historical Printing' is organised. During the conference, the process of making paper at the rate of 2000 sheets per day can be experienced within the short tours at the UICB Research and Production Paper Facility; also, tours to local Iowa City book artist and community studios and a visit to Route 3 Press producing the Wapsipinicon Almanac are offered. Finally, a post-conference walk around Iowa City observing lettering in the urban environment can be joined.

Fall Conference 2018

Cleveland, Ohio, USA
29–31 October 2018

The 2018 theme of the Fall Conference of FTA (Flexographic Technical Association) is "Taking Care of Business" – from how a company communicates and manages expectations to how it executes predictable, consistent and repeatable print. The topics of technical sessions are the flexography markets, workflow efficiency techniques, quality compliance, colour reproduction, effective customer communication, proper colour communication, and ink transfer, complemented by a panel discussion on the unique leadership styles.

WCPC Annual Technical Conference 2018

Swansea, UK
5 November 2018

Unlike the previous editions, the 14th Annual Technical Conference of WCPC (Welsh Centre for Printing and Coating) is announced as a one-day event. The agenda includes the sessions focused on rheological characterisation, printed sensors, functional printing and battery technology. The presentations deal with the effects of plasma functionalization on the print performance and time stability, tailored ink rheology, low-cost solutions for urban air quality management, hybrid coatings to develop barrier and antimicrobial properties for active packaging applications, expanded gamut optimisation for UV flexographic inks, formulation of NASICON (sodium superionic conductor) as a solid electrolyte for a sea-water open-cathode battery, carbon coatings as protective layers for current collectors, and more.

Graphic arts students can take part in Tom Frecska Student Printing Competition Award, presented by the Academy of Screen and Digital Printing Technology (ASDPT).

ICC Color Symposium

Hong Kong
22 October 2018

The topics of this symposium held at the Advanced Printing Technology Centre cover colour management techniques in digital workflows, including digital printing on textiles, the latest technology for soft proofing, colour communication in different stages of packaging production, standards in colour specification and colour appearance consistency. The ICC Meeting then takes place in Tokyo, Japan on 24–25 October.

CIDAG
5th International Conference in Design and Graphic Arts

Lisbon, Portugal
24–26 October 2018

The fifth edition of this biannual event is dedicated to design, graphic production, digital communication, including web design, ergonomics, usability and interactivity, and also the issues such as sustainability, inclusiveness, ethics or teaching.

6th International Printing Technologies Symposium

Istanbul, Turkey
1–3 November 2018

The International Printing Technology Symposium celebrates its 15th year in 2018. The participation at the sixth edition of the symposium hosted by the Istanbul University is free. The announced presentations mostly deal with digital printing, especially the inkjet technology. The combination of printing and digital technologies is represented also by the contribution focused on augmented reality.

ERA Packaging & Decorative Conference

Turin, Italy
7–8 November 2018

The 2018 conference of the European Rotogravure Association focused on packaging and decorative printing includes presentations on innovative gravure technology for short runs, novel drying technology, carbon fibre rollers, digital printing developments and also the draft of ISO 22909 standard describing the preparation of laminate samples for appearance assessment, among others. The visit to the plant of a large transfer printer is organised on the second day.

10th Workflow Symposium

Stuttgart, Germany
15 November 2018

This event covers JDF, Industry 4.0 and workflow automation. Besides the overview of advances related to these topics and live demonstrations of products, also the presentation discussing the importance of standardization in print and the role of the Ghent Workgroup is scheduled. Participation is free.

The Holography Conference

Minsk, Belarus
15–16 November 2018

This year's programme of the global conference for the commercial holography industry organised by Reconnaissance presents the developments in UV embossing technology and hologram converting, new advances in optical security features, novel applications of high-end mastering techniques, methods for the authenticity control of secure holograms, a study of forensic examination of hologram, and more.

CIC26 – 26th Color and Imaging Conference
Color Science and Engineering Systems, Technologies, and Applications

Vancouver, Canada
12–16 November 2018

Keeping the traditional schedule, the first two days of this annual conference sponsored by the Society for Imaging Science and Technology are again reserved for the short course programme, including the one-day introductory course on colour and imaging, followed by the workshops dedicated to challenges and perspectives of virtual and augmented reality, the use of deep learning in colour imaging, and movie production with HDR technology. The new short courses for 2018 explore the role of colour science in smartphone imaging for brand protection and secure applications, present variational colour image enhancement inspired by the human vision, and explain colour fundamentals in LED lighting. Also, the co-located meetings of the International Commission on Illumination are held on Monday – the annual meeting of CIE Division 8 (Image Technology) and the meeting of its Technical Committee 8-16 (Consistency of colour appearance within a single reproduction medium).

The main programme with a number of technical oral and poster presentations begins on the third day with the opening keynote of Radhakrishna Achanta presenting 'A brief history of superpixels' which were introduced to address the need to reduce the processing burden posed by large images, image-stacks, and videos. The main focus of this talk is on three efficient superpixel segmentation algorithms, namely Simple Linear Iterative Clustering (SLIC), its variant called Simple Non-iterative Clustering (SNIC), and an algorithm that relaxes the requirement of having roughly equal size as the third one. The keynotes for the next two days are 'Colour and consumer cameras: the good, the bad, the ugly' by Michael Brown, discussing the colour output of commodity cameras, common incorrect assumptions regarding image colour in the scientific literature and recent developments helping to improve the situation, and 'High Dynamic Range on the big screen' by Anders Ballesta. The CIC26 Evening Talk of Andrea Chlebak entitled 'Color in Narrative' and describing the process of coming to a final look for a film is scheduled on Wednesday. The same day, also the informal meeting on expanded gamut printing convened by Abhay Sharma is announced during the morning coffee break.

Image Processing and Communications

Bydgoszcz, Poland
14–16 November 2018

In 2018, the anniversary 10th International Conference on Image Processing & Communications organized by the Institute of Telecommunications, UTP University of Science and Technology is held. The three main areas of interest are computer vision, covering e.g. object recognition, image motion analysis, image and video coding, scene understanding and multimedia application, image analysis with topics such as image compression, character and documents analysis, image retrieval and image processing applications, and communications, including different types of networks, quality of service, new services and network reliability, among others.

Call for papers

The Journal of Print and Media Technology Research is a peer-reviewed periodical, published quarterly by iarigai, the International Association of Research Organizations for the Information, Media and Graphic Arts Industries.

JPMTR is listed in Emerging Sources Citation Index, Scopus, Index Copernicus International, PiraBase (by Smithers Pira), Paperbase (by Innventia and Centre Technique du Papier), NSD – Norwegian Register for Scientific Journals, Series and Publishers, and ARRS – Slovenian Research Agency, List of Scientific Journals.

Authors are invited to prepare and submit complete, previously unpublished and original works, which are not under review in any other journals and/or conferences.

The journal will consider for publication papers on fundamental and applied aspects of at least, but not limited to, the following topics:

- ### Printing technology and related processes
  Conventional and special printing; Packaging; Fuel cells, batteries, sensors and other printed functionality; Printing on biomaterials; Textile and fabric printing; Printed decorations; 3D printing; Material science; Process control

- ### Premedia technology and processes
  Colour reproduction and colour management; Image and reproduction quality; Image carriers (physical and virtual); Workflow and management

- ### Emerging media and future trends
  Media industry developments; Developing media communications value systems; Online and mobile media development; Cross-media publishing

- ### Social impact
  Environmental issues and sustainability; Consumer perception and media use; Social trends and their impact on media

Submissions for the journal are accepted at any time. If meeting the general criteria and ethic standards of scientific publishing, they will be rapidly forwarded to peer-review by experts of relevant scientific competence, carefully evaluated, selected and edited. Once accepted and edited, the papers will be published as soon as possible.

There is no entry or publishing fee for authors. Authors of accepted contributions will be asked to sign a copyright transfer agreement.

Authors are asked to strictly follow the guidelines for preparation of a paper (see the abbreviated version on inside back cover of the journal).

Complete guidelines can be downloaded from: <http://www.iarigai.org/publications/journals/>
Papers not complying with the guidelines will be returned to authors for revision.

Submissions and queries should be directed to: journal@iarigai.org

Vol. 7, 2018
Prices and subscriptions

Since 2016, the journal is published in digital form.
A print version is available on-demand and at additional price.

Please, find below the prices charged for the Journal, as well as for a single paper.
Use the opportunity to benefit from the Subscriber's discount price.

By ordering a publication, or by subscription, a password will be provided to you for downloading.
The password protection of every issue is active during a period of six months.
After this period the publications will be available free of charge.

iarigai members will be given the download password for free.

Regular prices

Four issues, digital JPMTR (password protected)	300 EUR
Single issue, digital JPMTR (password protected)	100 EUR
Single paper from JPMTR (PDF file)	20 EUR
Four issues, print JPMTR (on-demand)	400 EUR
Single issue, print JPMTR (on-demand)	100 EUR

Subscription prices

Annual subscription, four issues, digital JPMTR (password protected)	240 EUR
Annual subscription, four issues, print JPMTR (on-demand)	400 EUR

Prices for iarigai members

Four issues, digital JPMTR (password protected)	Free of charge
Single paper from JPMTR (PDF file)	Free of charge
Four issues, print JPMTR (on-demand)	400 EUR
Single issue, print JPMTR (on-demand)	100 EUR

Place your order online at: <http://www.iarigai.org/publications/subscriptions-orders/>
Or send an e-mail order to: office@iarigai.org

Guidelines for authors

Authors are encouraged to submit complete, original and previously unpublished scientific or technical research works, which are not under reviews in any other journals and/or conferences. Significantly expanded and updated versions of conference presentations may also be considered for publication. In addition, the Journal will publish reviews as well as opinions and reflections in a special section.

Submissions for the journal are accepted at any time. If meeting the general criteria and ethical standards of the scientific publication, they will be rapidly forwarded to peer-review by experts of high scientific competence, carefully evaluated, and considered for selection. Once accepted by the Editorial Board, the papers will be edited and published as soon as possible.

When preparing a manuscript for JPMTR, please strictly comply with the journal guidelines. The Editorial Board retains the right to reject without comment or explanation manuscripts that are not prepared in accordance with these guidelines and/or if the appropriate level required for scientific publishing cannot be attained.

A – General

The text should be cohesive, logically organized, and thus easy to follow by someone with common knowledge in the field. Do not include information that is not relevant to your research question(s) stated in the introduction.

Only contributions submitted in English will be considered for publication. If English is not your native language, please arrange for the text to be reviewed by a technical editor with skills in English and scientific communications. Maintain a consistent style with regard to spelling (either UK or US English, but never both), punctuation, nomenclature, symbols etc. Make sure that you are using proper English scientific terms. Literal translations are often wrong. Terms that do not have a commonly known English translation should be explicitly defined in the manuscript. Acronyms and abbreviations used must also be explicitly defined. Generally, sentences should not be very long and their structure should be relatively simple, with the subject located close to its verb. Do not overuse passive constructions.

Do not copy substantial parts of your previous publications and do not submit the same manuscript to more than one journal at a time. Clearly distinguish your original results and ideas from those of other authors and from your earlier publications – provide citations whenever relevant.

For more details on ethics in scientific publication consult Guidelines, published by the Committee on Publication Ethics (COPE): <https://publicationethics.org/resources/guidelines>

If it is necessary to use an illustration, diagram, etc. from an earlier publication, it is the author's responsibility to ensure that permission to reproduce such an illustration, diagram, etc. is obtained from the copyright holder. If a figure is copied, adapted or redrawn, the original source must be acknowledged.

Submitting the contribution to JPMTR, the author(s) confirm that it has not been published previously, that it is not under consideration for publication elsewhere and – once accepted and published – it will not be published under the same title and in the same form, in English or in any other language. The published paper may, however, be republished as part of an academic thesis to be defended by the author. The publisher retains the right to publish the printed paper online in the electronic form and to distribute and market the Journal containing the respective paper without any limitations.

B – Structure of the manuscript
Preliminary

Title: Should be concise and unambiguous, and must reflect the contents of the article. Information given in the title does not need to be repeated in the abstract (as they are always published jointly), although some overlap is unavoidable.

List of authors: I.e. all persons who contributed substantially to study planning, experimental work, data collection or interpretation of results and wrote or critically revised the manuscript and approved its final version. Enter full names (first and last), followed by the present address, as well as the E-mail addresses. Separately enter complete details of the corresponding author – full mailing address, telephone number, and E-mail. Editors will communicate only with the corresponding author.

Abstract: Should not exceed 500 words. Briefly explain why you conducted the research (background), what question(s) you answer (objectives), how you performed the research (methods), what you found (results: major data, relationships), and your interpretation and main consequences of your findings (discussion, conclusions). The abstract must reflect the content of the article, including all keywords, as for most readers it will be the major source of information about your research. Make sure that all the information given in the abstract also appears in the main body of the article.

Keywords: Include three to five relevant scientific terms that are not mentioned in the title. Keep the keywords specific. Avoid more general and/or descriptive terms, unless your research has strong interdisciplinary significance.

Scientific content

Introduction and background: Explain why it was necessary to carry out the research and the specific research question(s) you will answer. Start from more general issues and gradually focus on your research question(s). Describe relevant earlier research in the area and how your work is related to this.

Methods: Describe in detail how the research was carried out (e.g. study area, data collection, criteria, origin of analyzed material, sample size, number of measurements, equipment, data analysis, statistical methods and software used). All factors that could have affected the results need to be considered. Make sure that you comply with the ethical standards, with respect to the environmental protection, other authors and their published works, etc.

Results: Present the new results of your research (previously published data should not be included in this section). All tables and figures must be mentioned in the main body of the article, in the order in which they appear. Make sure that the statistical analysis is appropriate. Do not fabricate or distort any data, and do not exclude any important data; similarly, do not manipulate images to make a false impression on readers.

Discussion: Answer your research questions (stated at the end of the introduction) and compare your new results with published data, as objectively as possible. Discuss their limitations and highlight your main findings. At the end of Discussion or in a separate section, emphasize your major conclusions, pointing out scientific contribution and the practical significance of your study.

Conclusions: The main conclusions emerging from the study should be briefly presented or listed in this section, with the reference to the aims of the research and/or questions mentioned in the Introduction and elaborated in the Discussion.

Note: Some papers might require different structure of the scientific content. In such cases, however, it is necessary to clearly name and mark the appropriate sections, or to consult the editors. Sections from Introduction until the end of Conclusions must be numbered. Number the section titles consecutively as 1., 2., 3., ... while subsections should be hierarchically numbered as 2.1, 2.3, 3.4 etc. Only Arabic numerals will be accepted.

Acknowledgments: Place any acknowledgements at the end of your manuscript, after conclusions and before the list of literature references.

References: The list of sources referred to in the text should be collected in alphabetical order on at the end of the paper. Make sure that you have provided sources for all important information extracted from other publications. References should be given only to documents which any reader can reasonably be expected to be able to find in the open literature or on the web, and the reference should be complete, so that it is possible for the reader to locate the source without difficulty. The number of cited works should not be excessive - do not give many similar examples.

Responsibility for the accuracy of bibliographic citations lies entirely with the authors. Please use exclusively the Harvard Referencing System. For more information consult the Guide to Harvard style of Referencing, 6th edition, 2016, used with consent of Anglia Ruskin University, available at: <https://libweb.anglia.ac.uk/referencing/files/Harvard_referencing_201718.pdf>

C – Technical requirements for text processing

For technical requirement related to your submission, i.e. page layout, formatting of the text, as well of graphic objects (images, charts, tables etc.) please see detailed instructions at: <http://www.iarigai.org/publications/journals/>

D – Submission of the paper and further procedure

Before sending your paper, check once again that it corresponds to the requirements explicated above, with special regard to the ethical issues, structure of the paper as well as formatting.

Once completed, send your paper as an attachment to: journal@iarigai.org

If necessary, compress the file before sending it. You will be acknowledged on the receipt within 48 hours, along with the code under which your submission will be processed.

The editors will check the manuscript and inform you whether it has to be updated regarding the structure and formatting. The corrected manuscript is expected within 15 days.

Your paper will be forwarded for anonymous evaluation by two experts of international reputation in your specific field. Their comments and remarks will be in due time disclosed to the author(s), with the request for changes, explanations or corrections (if any) as demanded by the referees.

After the updated version is approved by the reviewers, the Editorial Board will decide on the publishing of the paper. However, the Board retains the right to ask for a third independent opinion, or to definitely reject the contribution.

Printing and publishing of papers, once accepted by the Editorial Board, will be carried out at the earliest possible convenience.

3-2018

The journal is publishing contributions
in the following fields of research

- Printing technology and related processes
- Premedia technology and processes
- Emerging media and future trends
- Social impacts

For details see the Mission statement inside

JPMTR is listed in

- Emerging Sources Citation Index
- Scopus
- Index Copernicus International
- PiraBase (by Smithers Pira)
- Paperbase (by Innventia and
  Centre Technique du Papier)
- NSD – Norwegian Register for
  Scientific Journals, Series and Publishers
- ARRS – Slovenian Research Agency,
  List of Scientific Journals

Submissions and inquiries

journal@iarigai.org

Subscriptions

office@iarigai.org

More information at

www.iarigai.org/publications/journal